APPENDIX E

SURFACE EMISSIONS,
REMOTE MONITORING STUDIES

SURFACE EMISSIONS, REMOTE MONITORING STUDIES

Prepared for:

U.S. Environmental Protection Agency
Air Pollution Prevention and Control Division
Air Pollution Branch
Research Triangle Park, NC 27711

Contract No. 68-C99-201
Work Assignment No. 4-003
Project No. RN992014.0003

Prepared by:

ARCADIS-Geraghty and Miller
P.O. Box 13109
Research Triangle Park, North Carolina 27709

September 16, 2003

CONTENTS

Page

Appendices

CONTENTS (Continued)

TABLES

FIGURES

CONTENTS (Continued)

FIGURES

Fugitive Gas Emission Measurements

Landfill gas emissions have been found to be a concern to human health and the environment due to the explosive potential of the gas, emissions of hazardous air pollutants (HAPs) and volatile organic compounds (VOCs), emissions of methane that contribute to climate change, and odor nuisance associated with landfill gas. Landfills emit more than 100 nonmethane organic compounds (NMOCs) (EPA 1997 a and b). The majority of the NMOCs are VOCs which contribute to urban smog. Over thirty of the landfill gas NMOCs are classified as HAPs (EPA 2003). As a result, landfills are listed as a source as part of the Urban Air Toxic Strategy.

Due to the concerns for human health and the environment, Clean Air Act (CAA) regulations have been promulgated that require landfill gas collection and control at landfills that (1) contain at least 2.5 million megagrams (Mg) or 2.5 million cubic meters of waste and (2) emit 50 Mg per year or more of NMOCs (EPA, 1998) The landfill evaluated in this study has gas collection and control and a portion of the gas is used at a near-by industrial plant as boiler fuel (offsetting fossil fuel). The measurements presented in this section are part of a larger effect by EPA's Office of Research and Development to obtain necessary data needed to update the existing set of landfill gas emissions factors (Thorneloe, 2003). These data will also be used to update the existing set of landfill gas emission factors and as input to the evaluation of residual risk from MSW landfills as required by CAA Section 112 (f).

Fugitive gas emissions are those emissions that are not captured for collection and control. Differences in how a site may be operated can contribute to the level of fugitive emissions. Optical remote sensing (ORS) was used to evaluate fugitive gas emissions for the retrofit and as-built bioreactors. Fugitive gas emissions have been identified as a potential concern because of the rapid increase in emissions when wet or bioreactor landfills are operated. The data collected through these field test measurements will help to evaluate these concerns and hopefully provide needed data to compare emissions from the as-built and retrofit bioreactors to the control site. Measurements were also conducted at the biocover units (where compost is used as a cover material) and compost facility.

At least 3 rounds of fugitive emissions testing are being conducted at this site to help evaluate any increase or decrease in emissions from bioreactors (as compared to conventional landfilling practice). This section provides the results from the first round of testing. The second and third rounds will be completed by the fall of 2003 with results available by spring of 2004. The data resulting from these field tests will be used along with other available data from operating bioreactors to update existing EPA emissions factors. Current factors do not consider operation under wet or bioreactor conditions. Sites that are not subject to CAA regulations either due to their size or mass emission rate are not required by federal regulations to collect and control landfill gas emissions. There has been a marked increased in interest and operation of landfills with leachate recirculation and other liquid additions. Many of these sites do not have gas collection and control. Data from this site will help to provide data needed to estimate emissions at sites without controls in place and determine what level of fugitives may exist for this type of operation.

Data from this site will also be used in EPA's MSW Decision Support Tool (DST) to quantify total emissions for both conventional and bioreactor operations to help provide perspective of the total emissions released to the environment over the length of time that emissions are released.

(Thorneloe, 2003) Offsets for landfill gas energy utilization will be accounted for along with emissions associated with the design, construction, operation, and monitoring of the landfill. The result will be an evaluation of the life-cycle environmental tradeoffs to compare wet landfills versus conventional landfills.

Figure 1 identifies each of the areas included in this study. The following tasks were conducted in September 2002 for the as-built and retrofit bioreactors and the control, bio-cover, and composting facility:

- Conduct background measurements using the bistatic open path-Fourier Transform Infrared Spectroscopy (OP-FTIR).

- Collect OP-FTIR data in order to identify major emissions hot spots by generating surface concentration maps in the horizontal plane using OP-FTIR spectrometer;

- Conduct vertical scans to determine the emission fluxes of detectable compounds downwind from major hot spots

- Collect ancillary data needed for calculating mass emissions rates for pollutants of concern including methane, VOCs, and HAPs. Data for ammonia emissions were collected for the compost facility and other areas.

- The following sections present an overview of:

    1. Optical remote sensing and calculation of emission flux;
    2. Data quality objectives and criteria;
    3. Round 1 field activities and data collection/analysis;
    4. Data Quality Assurance and Control; and
    5. Conclusions.

Optical Remote Sensing and Overview of Calculation of Emission Flux

The application of optical remote sensing (ORS) to quantify fugitive gas emissions has seen dramatic improvements over the last year partly due to the partnership between EPA's Emissions Measurement Center and the National Risk Management Research Laboratory (NRMRL). In addition, EPA's Environmental Technology Initiative has tested different instrument types to provide additional validation of new ORS instruments. Because of the advancements made with this technology, the Agency recommends that this be used for evaluating large area sources. ASTM procedures are available for application of open-path Fourier Transform Infrared (OP-FTIR) (ASTM E 1865-97, Re-approved 2002). The EPA's Emissions Measurement Center is working to develop an EPA test method for ORS to be available by fall 2004.

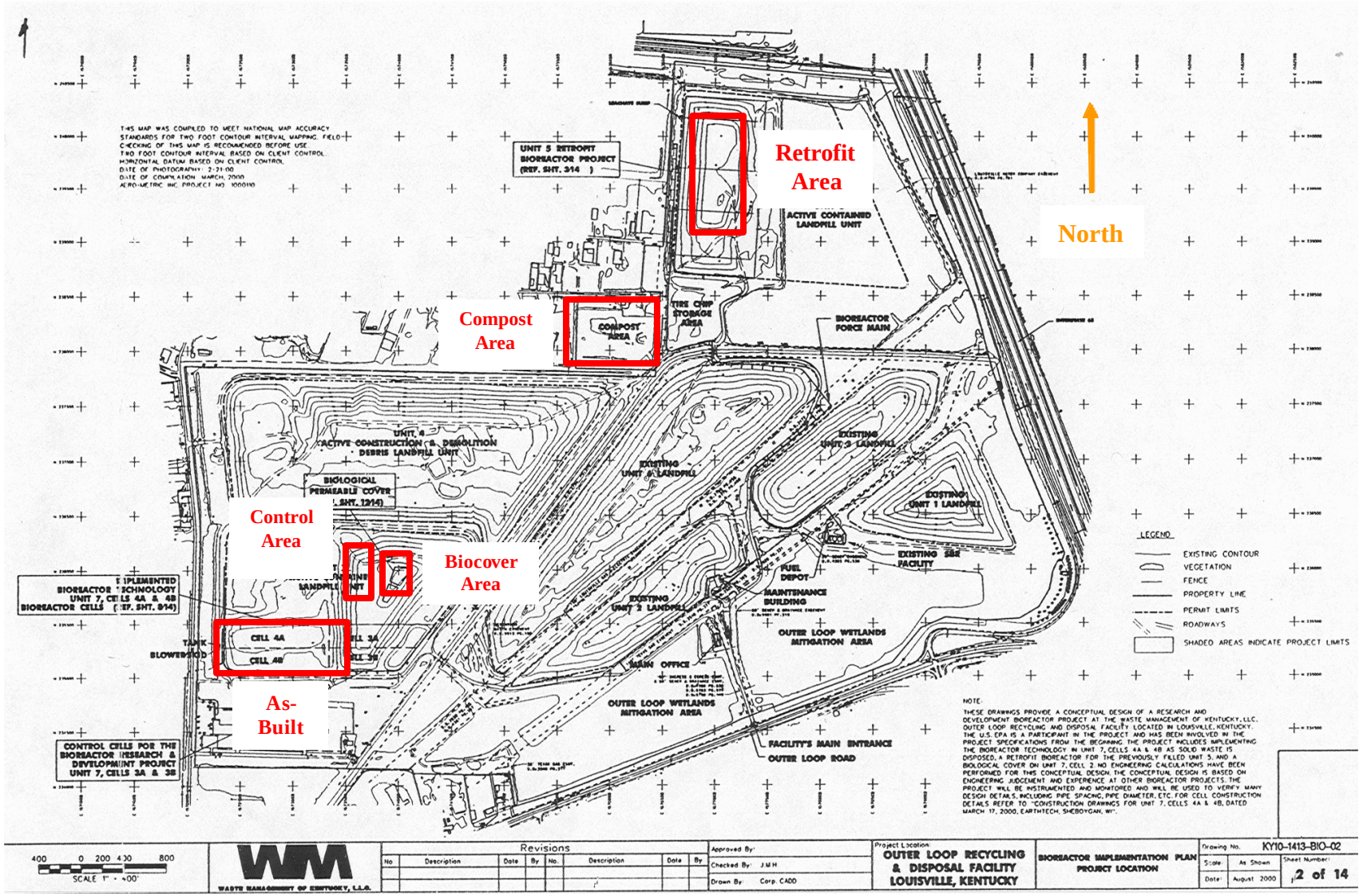

Figure 1. Waste Management, Inc. Outer Loop Facility Louisville, KY

The ORS improvements include an innovative method [Yost and Hashmonay, 2003] designed to obtain detailed spatial information from path-integrated ORD measurements by the use of optimization algorithms. The method uses a novel configuration of non-overlapping radial beam geometry to map the concentration distributions in a plane. This method, Radial Plume Mapping (RPM), is also applied to the vertical plane, downwind from the area source to map the crosswind and vertical profiles of a plume. The flux rate is calculated using wind data and other meteorological data. Measurements of any background emissions are also accounted for in these calculations through use of a bistatic Open-Path Fourier Transform Infra-red (OP-FTIR) instrument which can accurately measure the concentrations of a multitude of infrared absorbing gaseous chemicals with high temporal resolution. The chemical vapor, emitted from an emission source, forms a plume, which is carried by the wind across the multiple infrared beams. The beam measurements avoid some of the uncertainties that are inherent in the traditional point measurements. More information on these methods can be found in *Hashmonay and Yost* [1999B], and *Hashmonay et al*. [1999].

The OP-FTIR Spectrometer combined with the RPM method is designed for both fence-line monitoring applications, and real-time, on-site, remediation monitoring and source characterization. The OP-FTIR can be operated in either a monostatic, or bistatic configuration. In the monostatic configuration, an infrared light beam, modulated by a Michelson interferometer is transmitted from a single telescope to a retro reflector (mirror) target, which is usually set up at a range of 100 to 500 meters. The returned light signal is received by the single telescope and directed to a detector. The light is absorbed by the molecules in the beam path as the light propagates to the retro reflector and again as the light is reflected back to the analyzer. Thus, the round-trip path of the light doubles the chemical absorption signal.

In the bistatic configuration, the OP-FTIR detector, interferometer, and receiving optics are set up at one end of the path length being surveyed, and an infrared light source is set up at the other end of the path length. Generally, the path length is between 100 to 300 meters. In this configuration, light is absorbed by gas molecules as the light travels from the infrared source to the detector (once through the plume). The use of retro reflectors is not required when operating a bistatic OP-FTIR. A theodolite is used to make the survey measurement of the azimuth and elevation angles and the radial distances to the retro reflectors, relative to the OP-FTIR sensor.

Surface Radial Plume Mapping

This technique yields information on the two-dimensional distribution of the concentrations in the form of chemical-concentration contour maps (Hashmonay et al., 1999; Wu et al., 1999; Hashmonay et al., 2002). Horizontal radial scanning was performed with the ORS beams located as close to the ground as practical. This enhances the ability to detect minor constituents emitted from the ground, since the emitted plumes dilute significantly at higher levels above the ground. The survey area is divided into a Cartesian grid of ‘n’ times ‘m’ rectangular cells. A retro reflector is located in each of these cells and the OP-FTIR sensor scans to each of these retro reflectors, dwelling on each for a set measurement-time (30 seconds was used for this study). The system scans to the retro reflectors in the order of either increasing or decreasing azimuth angle. The path-integrated concentrations measured at each retro reflector are averaged over a several scanning cycles to produce time-averagedconcentration maps. Meteorological measurements were made concurrent to the scanning measurements.

For the first stage of reconstructing the average cell concentrations, an iterative algebraic deconvolution algorithm is used. The path-integrated concentration (PIC), as a function of the field of concentration, is given by:

$$PIC_k = \sum_m K_{km} c_m$$

where K is a Kernel matrix that incorporates the specific beam geometry with the cell dimensions; k is the number index for the beam paths and m is the number index for the cells; and c is the average concentration in the m^{th} cell. Each value in the Kernel matrix K is the length of the k^{th} beam in the m^{th} cell; therefore, the matrix is specific to the beam geometry. To solve for the average concentrations (one for each cell) the Non Negative Least Squares (NNLS) was applied. The NNLS is similar to a classical least square optimization algorithm, but is constrained to provide the best fit of non-negative values. The NNLS algorithm was tested and compared to the relaxation multiplicative algebraic reconstruction technique (MART) program previously developed and used. Both algorithms gave very similar results when reached to the same maximal level of fit between the predicted PIC and the observed PIC but the NNLS was much faster. Therefore, the NNLS algorithm will be applied in this study. This iterative procedure proceeds until the difference of the criteria parameter between sequential steps drops below a very small threshold value (tolerance). Multiplying the resulted vertical vector of averaged concentration by the matrix K, yields the end vector of predicted PIC data.

The second stage of the plume reconstruction is interpolation among the nine points, providing a peak concentration not limited only to the center of the cells. We will use the triangle-based cubic interpolation procedure. To extrapolate data values beyond the peripheral cell centers and within the rectangle measurement domain, we will assign the concentration of each corner cell to the corresponding corner of the domain.

Figure 2 represents a typical horizontal RPM configuration. In this particular case, n = m = 3. The orange lines define the nine cells in the matrix. The blue lines represent the 9 optical paths, each terminating at a retroreflector (Hashmonay et al., 2002). The red spot represents a point source. The enclosed areas represent the calculated plume, transported downwind by the wind. The numbers associated with the contour lines (isopleths) are the determined values for the concentrations.

Vertical Scanning

The RPM method maps the concentrations in the plane of the measurement. By scanning in a vertical plane downwind from an area source, plume concentration profiles can be obtained, and plane-integrated concentrations can be calculated. The Smooth Beam Function Minimization (SBFM) reconstruction approach is used with a two-dimensional smooth basis function (bivariate Gaussian) in order to reconstruct the smoothed mass equivalent concentration map. The smoothed mass equivalent concentration map is reconstructed using ***Matlab*** (MathWorks). In the SBFM approach, a smooth basis function is assumed to describe the distribution of concentrations, and the search is for the unknown parameters of the basis function. Since our interest is in the plane integrated concentration and not the exact map of concentrations in the plane, we fit only one smoothed basis function (one bivariate Gaussian) to reconstruct the smoothed map.

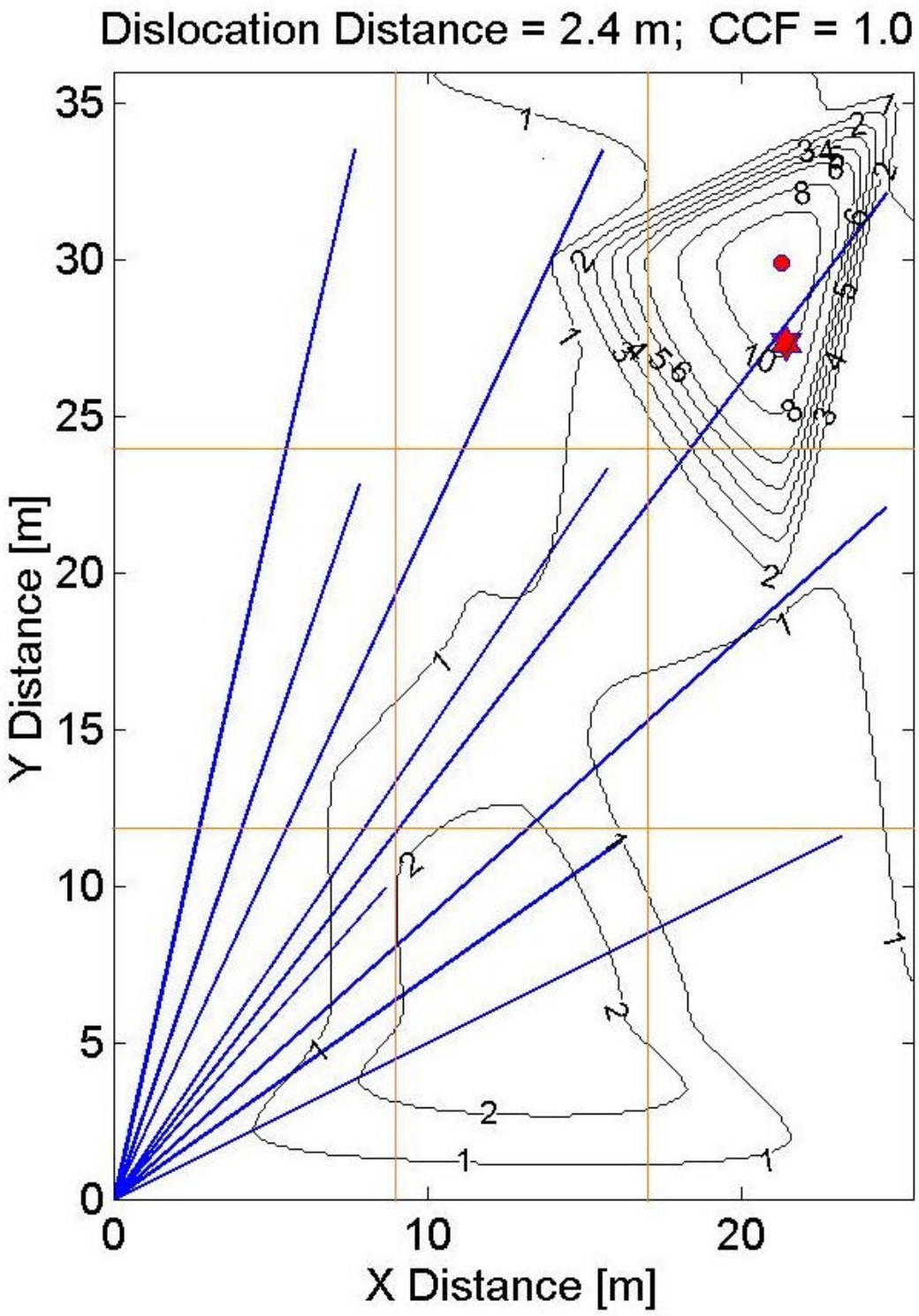

Figure 2. Example of a Typical Radial Scanning Configuration

However, this methodology does not assume that the true distribution of concentration in the vertical plane is a bivariate Gaussian. Earlier computational studies showed that one might fit a single bivariate Gaussian function to many kinds of skewed distribu-tions and still retrieve a reasonably good estimate of the plane-integrated concentration. The fit of a single bivariate Gaussian function to a multiple mode distribution was also examined and found that the reconstructed plane integrated concentration conserved fairly well the test input plane integrated concentration.

In each iterative step of the SBFM search procedure, the measured PIC values are compared with assumed PIC values, calculated from the new set of parameters. In order to compute the assumed PIC values, the basis function is integrated along the beam path's direction and path-length.

In our beam geometry, it is convenient to express the smooth basis function *G* in polar coordinates *r* and *è*.

$$G(r,q)=\frac{A}{2ps_y s_z\sqrt{1-r_{12}^2}}\exp\left\{-\frac{1}{2\left(1-r_{12}^2\right)}\left[\frac{(r\cdot\cos q-m_y)^2}{s_y^2}-\frac{2r_{12}\left(r\cdot\cos q-m_y\right)\left(r\cdot\sin q-m_z\right)}{s_y s_z}+\frac{\left(r\cdot\sin q-m_z\right)^2}{s_z^2}\right]\right\}$$

The bivariate Gaussian has six unknown independent parameters:

- *A* - normalizing coefficient which adjusts for the peak value of the bivariate surface
- $\tilde{n}_{12}$ - correlation coefficient which defines the direction of the distribution-independent variations in relation to the Cartesian directions *y* and *z* ($\tilde{n}_{12}$=0 means that the distribution variations overlap the Cartesian coordinates)
- m_y and m_z - peak locations in Cartesian coordinates
- and $\acute{o}_y$ and $\acute{o}_z$ - standard deviations in Cartesian coordinates. To fit the unknown parameters of the smooth basis function to the PIC data, one has to define an error function for minimization.

The Sum of Squared Errors (SSE) function is defined in our study as:

$$SSE\left(A, r_{12}, m_y, m_z, s_y, s_z\right)=\sum_i\left(PIC_i-\int_0^{r_i}G(r,q_i, A, r_{12}, m_y, m_z, s_y, s_z)dr\right)^2$$

Where *PIC* represents the measured PIC values and the index *i* is for the different beams. The SSE function is minimized using an iterative minimization procedure, such as the Simplex method, to solve for the unknown parameters. These calculations are performed using ***MatLab*** (MathWorks).

To obtain the plane-integrated concentration, we fit a bivariate Gaussian surface to match the volume under the underlying true concentration distribution surface. This volume is highly conserved in the fitting procedure, which emphasizes agreement over the five path integrals. Six independent beam paths are sufficient to determine one bivariate Gaussian that has six independent unknown parameters. This can be reduced to four setting the setting the correlation parameter $\tilde{n}_{12}$ equal to zero. This assumes that the reconstructed bivariate Gaussian is limited only to changes in the vertical and crosswind directions. In this case the above equation reduces to:

$$G(r,q)=\frac{A}{2ps_y s_z}\exp\left\{-\frac{1}{2}\left[\frac{(r\cdot\cos q-m_y)^2}{s_y^2}+\frac{(r\cdot\sin q-m_z)^2}{s_z^2}\right]\right\}$$

One also can fix the peak location in the vertical direction to the ground level when ground level emissions are known to exist, as in our field experiment. However, in this methodology, there is no requirement to apply a priori information on the source location and configuration.
Once the parameters of the function were found for a specific run, the concentration values are calculated for every square elementary unit in a vertical domain. These values are integrated incorporating wind speed data at each height level to compute the flux. In this stage, the concentration values are converted from parts per million by volume to grams per cubic meter, considering the molecular weight of the target gas and ambient temperature. The flux is calculated in grams per second, using wind speed data in meters per second. The flux leads directly to a determination of the emission rate (Hashmonay et al., 1998; Hashmonay and Yost, 1999A, Hashmonay et al., 2001). Thus, vertical scan leads to a direct measurement-based determination of the upwind source emission rate.
The Concordance Correlation Factor (CCF) is used to represent the level of fit for the reconstruction in the path-integrated domain (predicted vs. observed PIC). The CCF is similar to the Pearson correlation coefficient, but is adjusted to account for shifts in location and scale. Like the Pearson correlation, CCF values are bounded between -1 and 1, yet the CCF can never exceed the absolute value of the Pearson correlation factor. For example, the CCF will be equal to the Pearson correlation when the linear regression line intercepts the ordinate at 0, its slope equals 1. Its absolute value will be lower than the Pearson correlation when the above conditions are not met. For the purposes of this report, the closer the CCF value is to 1, the better the fit for the reconstruction in the path-integrated domain.
Figure 3 shows a schematic of the experimental setup used for vertical scanning. Several retro reflectors are placed in various locations on a vertical plane in-line with the scanning OP FTIR. The location of the vertical plane is selected so that it intersects the mean wind direction close to perpendicular as practical.

Virtual Flux Box

In concert with wind direction and speed data, the virtual flux box is an alternative ORS technique that yields emission fluxes. This technique is not as well developed as the vertical scanning technique. Conceptually, the virtual flux box may be regarded as three vertical planes (two beams per plane) such that

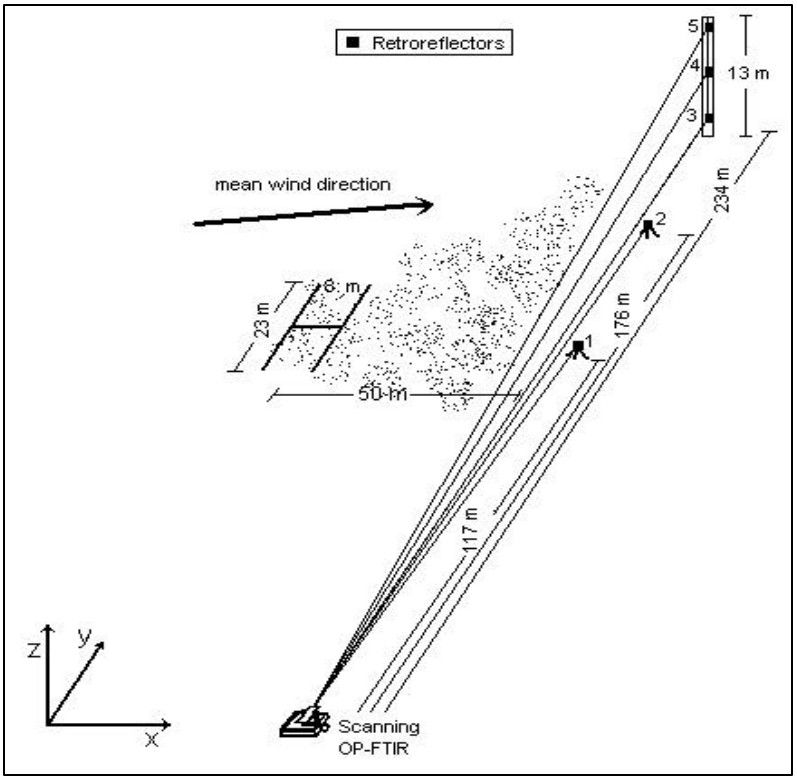

Figure 3. Example Vertical Scanning Configuration

the end points define the corners of the area under test. The virtual flux box was used at the Retrofit Area as backup data in case the vertical scanning configuration did not yield acceptable results (unfavorable wind directions).

Figure 4 illustrates the experimental setup for establishing a virtual flux box. This figure represents the installation of the scanning OP-FTIR in a virtual flux box configuration at an elevated site. The instrument, represented by the circle, is set up in the “southeast” corner. It scans to the retroreflectors (small square symbols) at six of the other seven corners of the virtual cubical box. The red lines represent the optical paths. By analogy to the vertical scanning configuration described previously, three small vertical planes are defined. Application of the SBFM function using a bivariate Gaussian model, will calculate the plume’s size. Emission fluxes are determined from the vertical-plane area-integrated concentration multiplied by the wind speed.

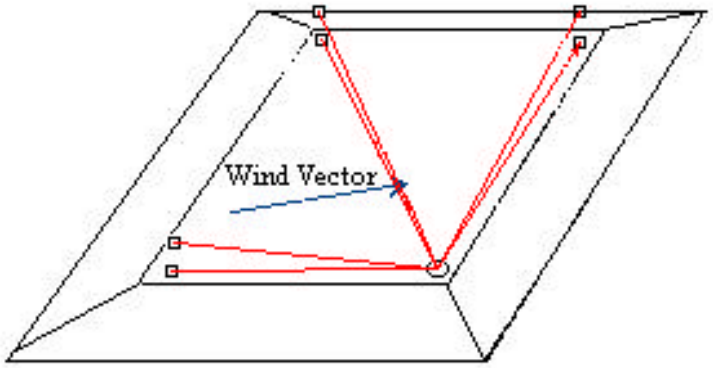

Figure 4. Example of Virtual Flux Box configuration

Data Quality Objectives and Criteria

Data quality objectives (DQOs) were developed using EPA's DQO Process (described in *EPA QA/G-4, Guidance for the Data Quality Objectives Process*) to clarify study objectives, define the appropriate type of data, and specify tolerable levels of potential decision errors that will be used as the basis for establishing the quality and quantity of data needed to support decisions. DQOs define the performance criteria that limit the probabilities of making decision errors by considering the purpose of collecting the data, defining the appropriate type of data needed, and specifying tolerable probabilities of making decision errors.

Quantitative objectives are established for critical measurements using the data quality indicators of accuracy, precision, and completeness. The acceptance criteria for these data quality indicators (DQI) are summarized in Table 1. Accuracy of measurement parameters is determined by comparing a measured value to a known standard. Values must be within the listed tolerance to be considered acceptable. Accuracy can also be measured by calculating the % bias of a measured value to that of a true value.

Precision is evaluated by making replicate measurements of the same parameter and by assessing the variations of the results. Replicate measurements are expected to fall within the tolerances shown in Table 1. Completeness is expressed as a percentage of the number of valid measurements compared to the total number of measurements taken.

Estimated minimum detection limits, by compound, are given in Table 2. It is important to note that the values listed in Table 2 are considered approximate. Minimum detection limits can vary based on atmospheric conditions. Minimum detection levels for each absorbance spectrum are determined by calculating the root mean square (RMS) absorbance noise in the spectral region of the target absorption feature. The minimum detection level is the absorbance signal (of the target compound) that is five times the RMS noise level, using a reference spectrum acquired for a known concentration of the target compound.

Table 1. DQI Goals for Critical Measurements

Measurement Parameter	Sampling Method(s)	Analysis Method	Accuracy	Precision	% Complete
Wind direction	N/A	Magnetic compass with vane	±5° tolerance	±5°	90%
Wind speed	N/A	Heavy duty wind cup set	±0.8 m/s	± 0.8 m/s	90%
Optical path-length	N/A	Theodolite	±1m	± 1 m	100%
Mid-IR absorbance	N/A	FTIR	±10%	± 10%	90%
Elemental Hg	N/A	Lumex	±20%	±20%	90%

Table 2. Detection Limits for Target Compounds

Compound	Sampling/Analytical Method	Est. Detect. Limit for Path Length = 100m, 1 min Ave. (ppmv)	AP-42 Value - Conc in raw landfill gas (ppmv)
Butane	FTIR	0.006	5.03
Carbonyl sulfide	FTIR	0.006	0.49
Chloromethane	FTIR	0.012	1.21
Dichlorodifluoromethane	FTIR	0.004	15.7
Dichlorofluoromethane	FTIR	N/A	2.62
Ethane	FTIR	0.010	889
Ethyl chloride	FTIR	0.004	1.25
Fluorotrichloromethane	FTIR	0.004	0.76
Methane	FTIR	0.024	N/A
Pentane	FTIR	0.008	3.29
Propane	FTIR	0.008	11.1
1,3-Butadiene	FTIR	0.012	N/A
Acetone	FTIR	0.024	7.01
Acrylonitrile	FTIR	0.010	6.33
Benzene	FTIR	0.040	N/A
Bromodichloromethane	FTIR	N/A	3.13
Carbon disulfide	FTIR	0.028	0.58
Carbon tetrachloride	FTIR	0.008	0.004
Chlorobenzene	FTIR	0.040	0.25
Chloroform	FTIR	0.012	0.03
Dimethyl sulfide	FTIR	0.018	7.82
Ethyl mercaptan	FTIR	N/A	2.28
Ethylene dibromide	FTIR	0.006	0.001
Ethylene dichloride	FTIR	0.030	0.41
Hexane	FTIR	0.006	6.57
Methyl chloroform	FTIR	0.006	N/A
Methyl isobutyl ketone	FTIR	0.040	1.87
Methylene chloride	FTIR	0.014	14.3
Propylene dichloride	FTIR	0.014	0.18
t-1,2-Dichloroethene	FTIR	N/A	2.84
Tetrachloroethene	FTIR	0.004	3.73
Toluene	FTIR	0.040	N/A
Trichlorethylene	FTIR	0.004	2.82
Vinyl chloride	FTIR	0.010	7.34
Vinylidene chloride	FTIR	0.014	0.20
Ethanol	FTIR	0.006	27.2
Methyl ethyl ketone	FTIR	0.030	7.09

Compound	Sampling/Analytical Method	Est. Detect. Limit for Path Length = 100m, 1 min Ave. (ppmv)	AP-42 Value - Conc in raw landfill gas (ppmv)
2-Propanol	FTIR	0.006	50.1
1,4-Dichlorobenzene	FTIR	0.012	0.21
Ethyl benzene	FTIR	0.060	4.61
Xylenes	FTIR	0.030	12.1
Hydrogen sulfide	FTIR	6.0	35.5
Methyl mercaptan	FTIR	0.060	2.49
Acetaldehyde	FTIR	0.010	N/A
Formaldehyde	FTIR	0.006	N/A

*N/A indicates that estimated minimum detection levels were not available for a particular compound.

*The AP-42 values represent an average concentration of different pollutants in the raw landfill gas. This is not comparable to the detection limits for the OP-FTIR, which is an average value for a path length of 100 meters across the surface of the area source being evaluated. However, it does provide an indication of the types of pollutants and range of concentrations associated with landfill gas emissions in comparison to the detection limits of the OP-FTIR.

Round 1

Field Activities and Data Collection

Field-testing was conducted as indicated in Table 3 during September of 2002. Data analysis was performed in the months of October 2002 through January 2003.

Magnifications of the areas identified in Figure 1 are provided for each field test location. Within these figures, circles indicate the locations of the bistatic instrument and source. The location of the scanner plus monostatic FTIR is indicated by a circle, and the location of the scissors jack is indicated by the square.

Theodolite measurements of the standard distance, and horizontal and vertical position of each retroreflector (mirror) were taken in each survey area. These measurements are presented in Tables A-1 to A-5 of Appendix A.

As-Built Area

Figure 5 shows the optical configurations used at the As-Built Area. Four surface non-scanning experiments were performed prior to the vertical scan due to limited access time at this site (we would have preferred to conduct a full radial scan). The results were used to determine concentrations of methane and VOCs but there was not enough data to construct a concentration contour map.

The vertical scanning configuration was set up along the southern boundary of the As-Built Area (see Figure 5), since the observed mean wind was from the northeast. Concurrent meteorological data was collected during these tests. Additionally, the bistatic FTIR instrument was operated along the western boundary of the AALB to collect background concentration data, since the prevailing wind direction was initially from the west-northwest.

Table 3. Schedule of ORS Measurements for Round 1

Date	Day of Week	Detail of Work Performed
Sept 5	Thursday	Travel to site
Sept 6	Friday	AM-Arrive at site PM-Begin Survey/Set-up Work
Sept 7	Saturday	Vertical Scanning of Compost Area
Sept 8	Sunday	Radial and Vertical Scanning of As-Built Area
Sept 9	Monday	Vertical Scanning of Biocover Area
Sept 10	Tuesday	Vertical Scanning of Control Area
Sept 11	Wednesday	Radial Scanning of Retrofit Area
Sept 12	Thursday	Vertical Scanning of Retrofit Area
Sept 13	Friday	AM-Virtual Flux Box Scanning of Retrofit Area PM-Travel from site

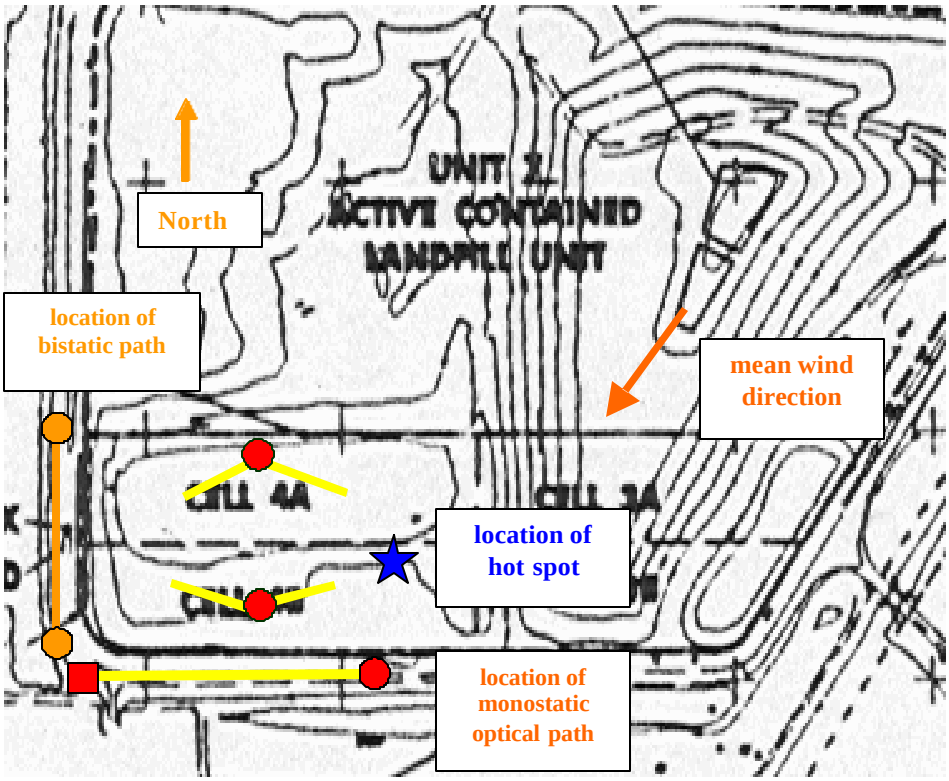

Figure 5. Map of As-Built Area showing Location of Vertical Plane, Surface Scanning, Background Measurements, and possible "Hot Spot

Retrofit Area

Vertical and horizontal scanning, as well as a virtual flux box configuration was performed at the Retrofit Area test site. Due to the size, dimensions, and collection system configuration of this site, separate experiments of each type were performed on the north and south "halves" of this plateau. Figure 6 shows the vertical configurations used at the Retrofit Area test site. Figure 7 presents the radial scanning configurations used at the Retrofit test site, as well as the location of ten gas extraction pipes observed at the site (denoted by red as well as the location of ten gas extraction pipes observed at the site (denoted by red circles). The locations used for the two vertical plane experiments were defined in permit applications to the FAA. Due to the site's elevation, proximity to the airport, and the scissor jack height when extended, FAA approval for narrowly defined scissor jack locations was required (North: 38°08'58" N, 85°43'14" W; South: 38°08'51" N, 85°43'14" W). Concurrent meteorological data was collected during these tests. USEPA personnel operated a non-scanning bistatic FTIR along the northern boundary of the Retrofit Area, since the prevailing wind direction was initially from the north.
Concurrent meteorological data was collected during these tests. USEPA personnel operated a non-scanning bistatic FTIR along the northern boundary of the Retrofit Area, since the prevailing wind direction was initially from the north.
.

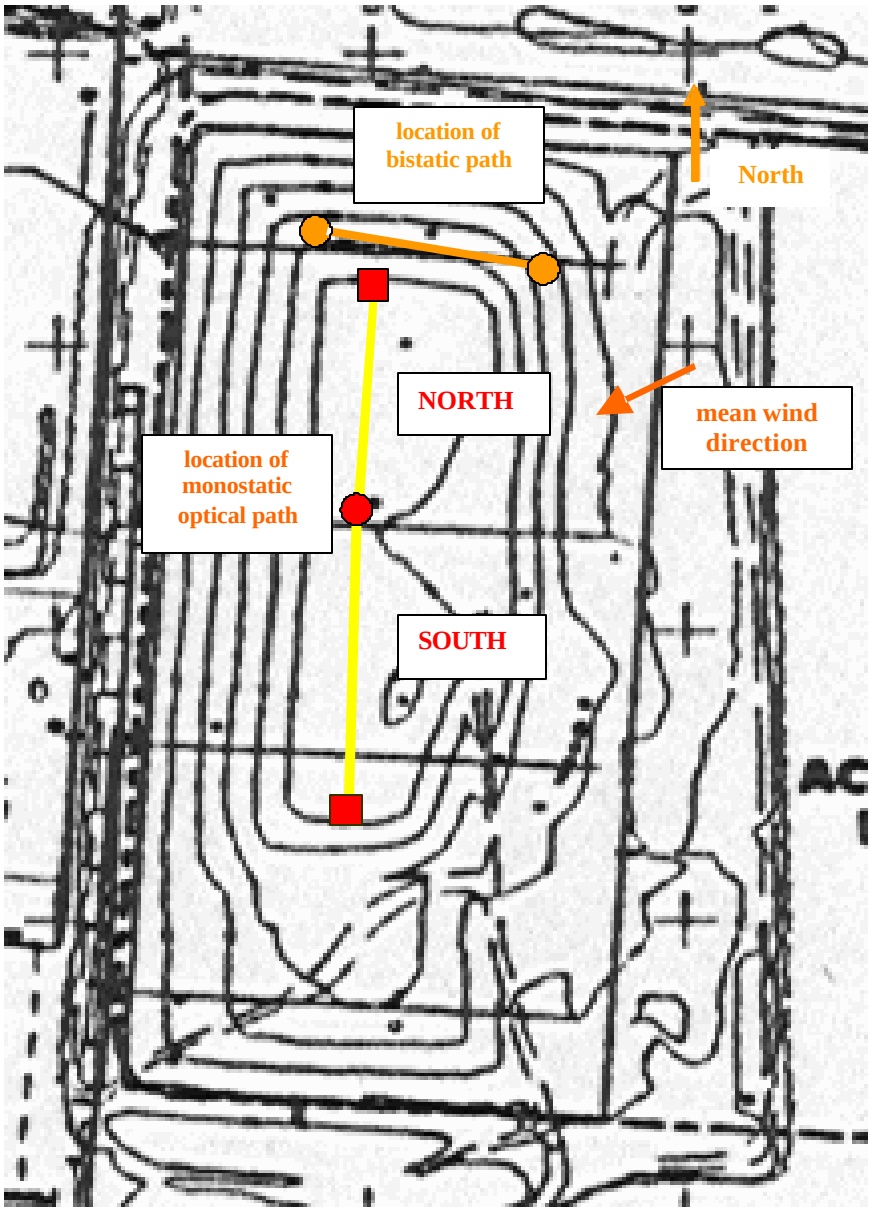

Figure 6. Map of Retrofit Area (North and South) showing Location of Vertical Planes and Background Measurements

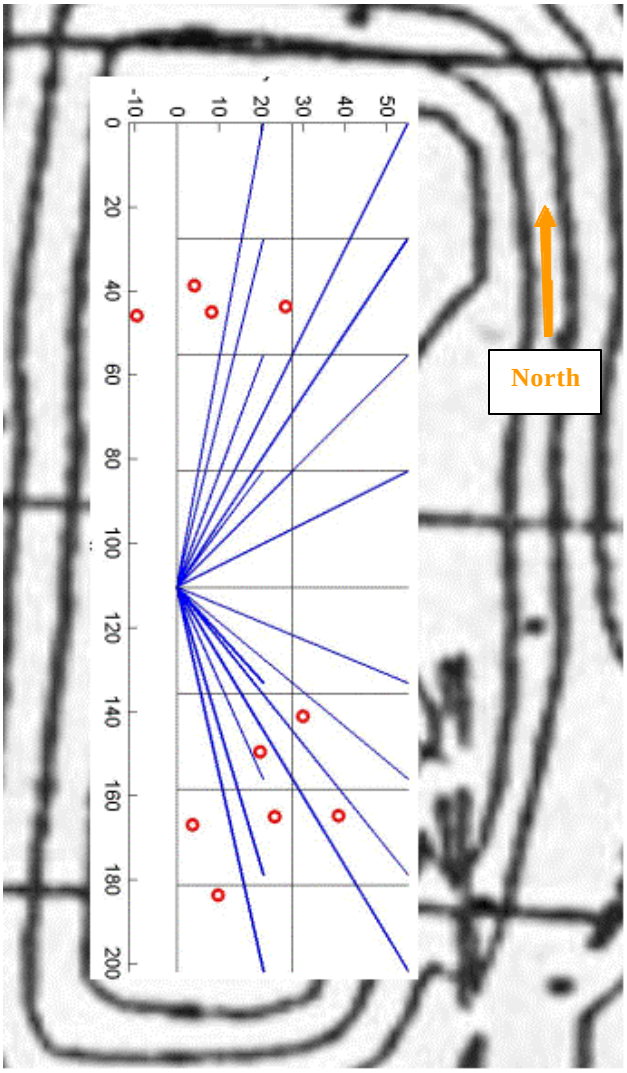

Figure7. Map of Retrofit Area (North and South) showing Location of Mirrors for Radial Scanning and Gas Extraction Pipes

Control Area

Figure 8 shows the vertical configuration used in the Control Area. As mentioned in Section 1.2.7, the Control Area chosen for the study was located north of the As-Built Area. The vertical configuration was set up on the east side of the Control Area, and data was collected during periods that westerly winds were observed at the test site.

Biocover Area

Figure 9 shows the Biocover Area test site. Vertical scan experiments were set up with four mirrors instead of five while the fifth mirror was used as a surface scan along the diagonal of the Biocover Area. The vertical configuration was located directly west of the actual test area (see Figure 9). The favorable wind direction for this configuration would consist of an easterly component. During the period of the survey, westerly, as well as easterly winds were observed at the test site. Actual emission data from the Biocover Area was gathered during periods of easterly winds. The Biocover test site represents a one-acre plot within a conventionally configured landfill.

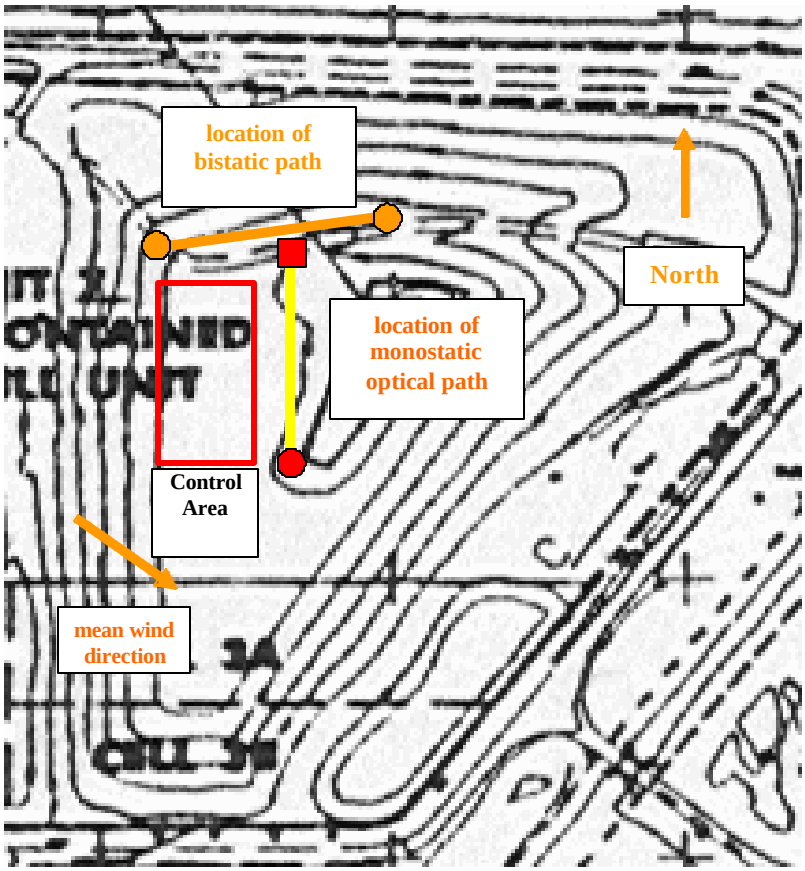

Figure 8. Map of Control Area showing Location of Vertical Plane and Background Measurements

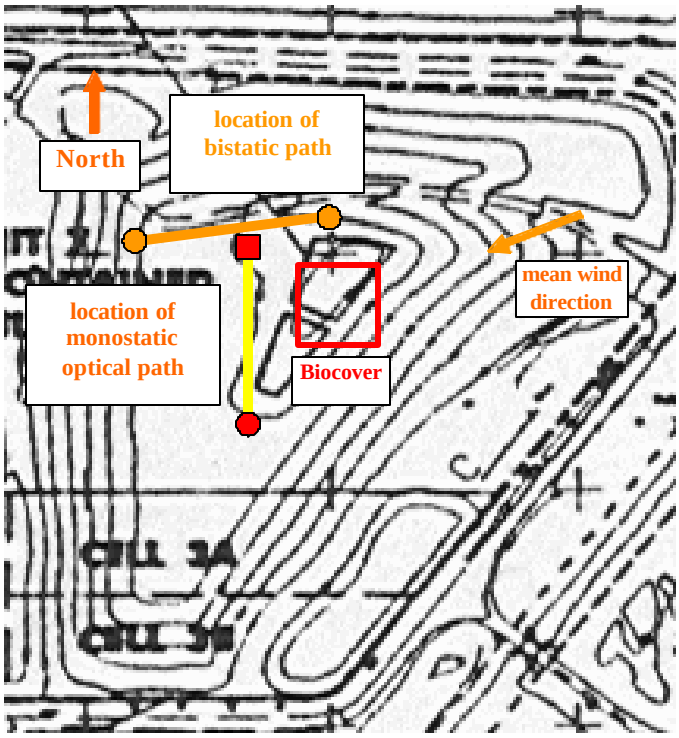

Figure 9. Map of Biocover Area showing Location of Vertical Plane and Background Measurements

Concurrent meteorological data was collected during these tests. A non-scanning bistatic FTIR was operated in an upwind location concurrent with these tests.

Compost Area

Figure 10 shows the Compost Area and the optical configurations used during testing. The large blue circles denote the locations of the compost piles surveyed. Two vertical scanning configurations were setup directly adjacent to two compost piles. It is important to note that physical barriers such as a fence line and the actual location of the compost piles configurations were setup directly adjacent to two compost piles. Physical barriers such as the fence line and the location of the compost piles limited the vertical configuration used for the survey. The winds during the time of the survey fluctuated, but were predominately oriented to the west-northwest. Since the vertical scanning configuration for pile 1 was oriented to the west of the pile, this scanning configuration was considered an upwind measurement.

The scanning configuration used to survey pile 2 was located east of the compost pile, so this was considered a downwind measurement. Concurrent meteorological data was collected during these tests. Background concentration data were collected along the eastern boundary of the Compost Area using the bistatic FTIR instrument.

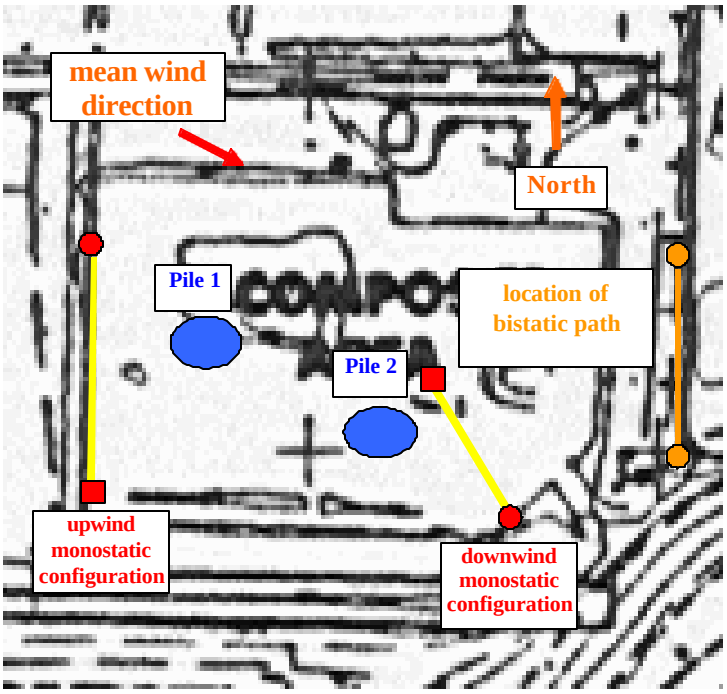

Figure 10. Map of Compost Area showing Locations of Vertical Planes and Location of Background Measurements

Data Analysis and Results

FTIR data were collected as interferograms. All data were archived to CD-ROMs. After archiving, interferograms were transferred to USEPA personnel who performed the transformations to absorbance spectra and then calculated concentrations using a combination of AutoQuant® (Midac) and Non-Lin® (Spectrosoft) quantification software. This analysis was done after completion of the field campaign. Concentration data were matched with the appropriate mirror locations, wind speed, and wind direction. MatLab® (Math-works) software was then used to process the data into horizontal plane concentration maps or vertical plane plume visualizations, as appropriate.

The fluxes are determined as the sum across the matrix of the point-wise multiplication of the concentrations times the wind speed. Emission fluxes for VOCs were calculated by proportioning to the methane flux.

Meteorological data including wind direction and wind speed were continuously collected during the sampling/measurement campaign with a Climatronics model 101990-G1 instrument. The Climatronics instrument is automated. It collects real-time data from its sensors and records time-stamped data as one-minute averages to a data logger. Wind direction and speed-sensing heads were used to collect data at 2 heights, nominally at 2 and 10 meters (the 10 meter sensor was placed on top of the scissors jack). The sensing heads for wind direction incorporate an auto-northing function (automatically adjusts to magnetic north) that eliminates the errors associated with subjective field alignment to a compass heading. The sensing heads incorporate standard cup-type wind speed sensors. Post-collection, the two sets of data were fit linearly to estimate wind velocity as a function of height.

Statistical analysis was performed on several of the data sets to assess data quality and consistency. Average fluxes reported are calculated in the following manner: (a measurement loop mentioned hereafter is a measurement cycle by scanning one time through all he mirrors in

the configuration.): Path-integrated concentration values from measurements made on each beam path (looking at the corresponding mirror) are averaged for four consecutive loops, which satisfy a specified condition for acceptable wind direction. The wind measurements are made at 2m and 10m above ground, and interpolated to six equidistant levels from 2m to 12m. The acceptable wind direction criterion is that the wind direction at 4m height must be within 70 degrees angle from the normal to the plane where the OP-FTIR measurements are made. The measurement plane is the plane in which all the mirrors and the OP-FTIR instrument are placed. All measurement loops which do not satisfy the above wind direction criterion are rejected. The wind speed and wind direction are averaged for our consecutive accepted loops similar to the path-integrated concentrations. A radial plume-mapping algorithm was used to compute the mass-equivalent plume image, and the flux in grams per second across the plane of the measurement. Ideally, one would like to have four loops (that are averaged) measured consecutively, which would be the case with consistent wind conditions. However, with unstable wind conditions and/or with wind directions close to 70 degrees from normal, some loops may be rejected in order to maintain data quality. For example, only 7 out of 16 loops shown in Table B-1 satisfy the wind criterion for the As-Built area, which is reported in Section 3.1. For measurements with more than four loops satisfying the wind criterion, a moving average is made with a grouping of four, and the flux across the measurement plane is calculated. In order to assess the accuracy of reconstruction for each moving average group, the Concordance Correlation Coefficient (CCF) has been computed for each reconstruction. The surface plume concentrations are calculated by calculating a path-integrated average for each pixel. Then, contour lines representing concentrations are drawn by interpolating between the nine average pixel values

As-Built Area

Table 4 presents the methane emission flux from the vertical scanning survey of the As-Built Area. A map of this site and the optical configurations are provided in Figure 5. The first column of this table refers to a running average calculation from the several loops of data collected. The second column shows the calculated CCF. The third, fourth, and fifth columns show the calculated methane flux (in grams per second), and the average wind speed and wind direction during the time the measurements were taken, respectively. The methane concentrations used to create this table can be found in Table B-1 of Appendix B.

Table 4. Moving average of calculated methane flux, CCF, wind speed, and wind direction* for the As-Built Area

Loops	CCF	Flux (g/s)	Wind Speed (m/s)	Wind Dir (deg)
1 to 4	0.980	165	1.91	51
2 to 5	0.977	180	2.38	33
3 to 6	0.962	168	2.52	36
4 to 7	0.958	118	2.15	43
Average	0.969	160		
Std. Dev. of Mean	0.0108	27.3		

*wind direction shown is the angle from a vector normal to the plane of the configuration

Figure 11 presents a map of the reconstructed methane plume from the As-Built vertical scanning survey. Contour lines give methane concentrations in ppm. The average calculated methane flux from the As-Built Area was 160 g/s.

In addition to measuring methane concentrations and methane flux, additional analysis was done to measure emissions of ammonia and VOCs from the As-Built Area. VOC concentrations and fluxes measured at the site were generally either too low to be detected, or were detected in only trace amounts. Consistent with the QAPP, emission concentrations and fluxes for these trace VOCs were calculated by proportioning to the methane concentration and flux.

It is known that methane comprises approximately 50% of landfill gas. Proportioning an estimated methane concentration of 500,000 ppmv to the highest methane concentration found at the site, and ratioing this to the AP-42 value for each target VOC (found in Table 2), it was found that the expected VOC concentrations were often below the estimated minimum detection limit for the target VOC. As mentioned in Section 2.5, this was anticipated prior to performance of the experiments.

Tables 5 and 6 present concentrations and calculated fluxes (in g/s) of VOCs and Ammonia measured during runs 1 and 2, respectively, of the AALB vertical scanning survey. The VOC fluxes were calculated by ratioing the measured methane concentrations with the measured VOC concentrations. For example, in Table 5, the average calculated methane flux value is 118 g/s. The average methane concentration is 109 ppmv. The average calculated ammonia flux is found by first multiplying the ratio of methane to ammonia concentration (109ppmv/ 0.0049ppmv) by the ratio of the molecular weight of methane to ammonia (16g/17g). This value (20,936.4) is then proportioned to the average calculated methane flux to yield the value of the average calculated ammonia flux (0.0056g/s).

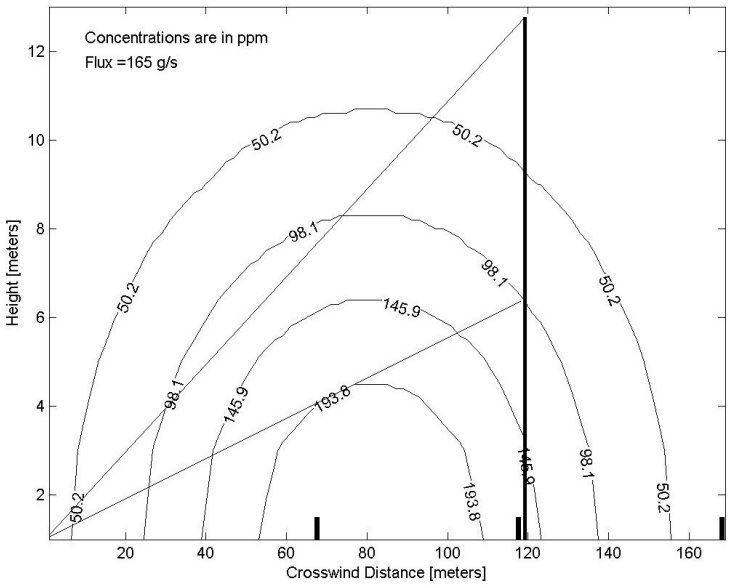

Figure 11. Reconstructed average methane plume from the moving average of loops 1 to 4 of the As-Built Vertical Scanning Survey

Table 5. Average Concentration and Calculated Flux of VOCs, Ammonia, and Methane for As-Built Vertical Scan-Run 1

Compound	Minimum Detection Level (ppmv)	Average Conc. (ppmv)	Flux (g/s)
MTBE*	0.0099	0.0602	0.33
Ammonia	0.0024	0.0049	0.0056
Straight-Chain Hydrocarbons	0.49	1.6	9.2
Bent-Chain Hydrocarbons	0.084	0.47	2.3
Methane		109	118

*MTBE= Methyl tert-butyl ether

Table 6. Average Concentration and Calculated Flux of VOCs for As-Built Vertical Scan-Run 2

NMOC	Minimum Detection Level (ppmv)	Avg. Concentration (ppmv)	Flux (g/s)
MTBE*	0.0098	0.018	0.102
Straight-Chain Hydrocarbons	0.48	0.85	5.1
Bent-Chain Hydrocarbons	0.27	0.95	4.8
Methane		147	165

As was reported above, the average calculated methane flux from the As-Built Area was 160 grams per second. However, this value may be a low estimate of the total methane flux from the As-Built Area. The observed wind direction during the vertical scanning survey was variable. Environments having variable wind directions are classified as unstable. Other studies have found that calculated fluxes could underestimate actual fluxes by as much as 35% in unstable environments [*Hashmonay et al.,* 2001]. Additionally, the axis of the vertical scanning configuration was oriented along the southern boundary of the As-Built Area (see Figure 5). However, due to limitations in the instrumentation, it was not possible for the vertical scanning configuration to include the entire southern boundary of the survey area. The optical range of the OP-FTIR instrument used in this study was approximately 200 meters, which is less than the total distance of the southern boundary of the As-Built Area. Because of this, it is possible that the entire methane plume from the As-Built was not captured by the vertical configuration. Consequently, the calculated methane flux from the
As-Built Area may be underestimating the actual flux, but the major identified “hot spot” was fully quantified.

Due to time constraints and instrument limitations discussed in Section 2.1, a complete radial scan of the As-Built Area was not performed to identify the exact location of “hot spots” which may have contributed to the calculated methane flux. However, a non-scanning surface survey was performed in the As-Built using 4 beams. This survey was done over the western and central areas of the As-Built Area (see Figure 5). Concentrations of various compounds (including

methane) were calculated from the four surface non-scanning experiments. The measured concentrations are presented in Tables B-2 to B-5 in Appendix B. Analysis of the wind data revealed that the prevailing wind direction during the vertical scanning survey was from the northeast. With this knowledge of the wind data, (and due to the fact that much lower methane concentrations were found during the surface survey of the western and central areas of the As-Built Area, along with data from the vertical scanning survey which gives plume shape and location with respect to relevant wind direction), we can conclude, based on the method described by *Hashmonay and Yost* [1999A], that any "hot spots" contributing to the methane fluxes calculated were probably located in the eastern portion of the As-Built Area (consisting of cells 4A and 4B). A blue star in Figure 5 of Appendix A denotes the location of this "hot spot".

3.2.2 Retrofit Area

As mentioned earlier, radial and vertical scanning were performed in the Retrofit area. The radial scanning was performed to identify methane "hot spots". Figure 12 presents a contour map of reconstructed methane concentrations (in ppm) from this area, and Table B-6 of Appendix B shows actual methane concentrations measured during radial scanning. The figure shows the presence of two distinct "hot spots", or areas where methane concentrations exceed 79 ppmv. The red circles show the locations of ten gas extraction pipes observed in the Retrofit Area. Tables 7 and 8 present methane emission flux determinations for the northern and southern halves of the Retrofit Area, respectively. The optical configurations for this site are provided in Figure 6. In Table B-7, the measured methane concentrations are provided from the vertical scanning monitoring. The first column of these tables refers to a running average calculation from the several "loops" of data collected. The second column shows the calculated CCF. The third, fourth, and fifth columns show the calculated methane flux (in grams per second), and the average wind speed and wind direction during the time the measurements were taken, respectively.

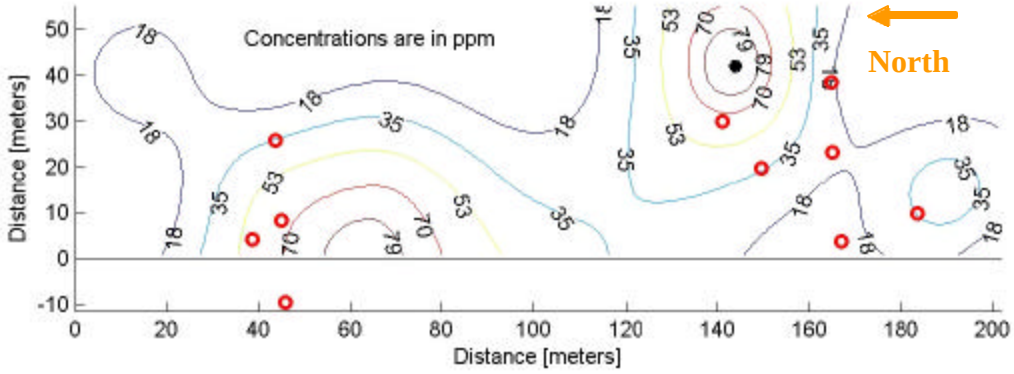

Figure 12. Reconstructed Methane Concentrations (in ppm) for the Retrofit North and South Areas

Table 7. Moving Average of Calculated Methane Flux, CCF, Wind Speed, and Wind Direction for the Retrofit North Area

Loops	CCF	Flux (g/s)	Wind Speed (m/s)	*Wind Dir. (deg)
1 to 4	0.980	19	3.14	355
2 to 5	0.987	18	3.29	356
Average	**0.983**	**19.0**		
Std. Dev. of Mean	**0.0049**	**0.707**		

*wind direction shown is the angle from a vector normal to the plane of the configuration

Figures 13 and 14 present the reconstructed methane plume from Retrofit North and South vertical scanning survey, respectively. Contour lines give methane concentrations in ppm. The average calculated methane flux for the northern half of the Retrofit Area was 19 grams per second, and the average calculated methane flux for the southern half was 20 grams per second. Two virtual flux box configurations were conducted in the Retrofit Area. The results from this showed consistent emissions results as was found using the vertical scanning measurements.
As mentioned earlier, Figure 12 shows that two distinct methane "hot spots" were found in the Retrofit Area. The peak methane concentrations found in each "hot spot" were similar (greater than 79 ppmv). One "hot spot" was located in the Retrofit North area, and one in the Retrofit South area. The proximity of these "hot spots" to the location of the gas extraction pipes (indicated by red circles), and analysis of wind data at the time of the measurements, suggests the pipes may be a significant source of methane emissions.
Closer inspection of the average reconstructed methane plumes from Retrofit North and South vertical scanning surveys (Figures 13 and 14, respectively) show that the average calculated methane fluxes for each area are very similar. This is not surprising, since the methane concentrations found in the "hot spots" for each area (which would be the major contributor to methane flux values) are similar in magnitude. Additionally, the spatial distribution of the plumes in the horizontal direction is consistent with the location of the "hot spots". The center of the Retrofit North "hot spot" is located about 45 meters north of the position of the scanner. Figure 13 shows that the center of the methane plume found in the Retrofit North area is located about 40 meters from the scanner position. The center of the Retrofit South "hot spot" is located about 30 meters south of the position of the scanner. Figure 14 shows that the center of the methane plume found in the Retrofit South area is located about 35 meters from the scanner position. It appears that there was very good agreement between the location of "hot spots" found during the radial surface scanning surveys, and the plume reconstruction done from the vertical scanning surveys.
Observed wind directions during the Retrofit vertical scanning surveys were stable. This would be indicative of a stable atmosphere. *Hashmonay et al.* [2001] found that fluxes calculated during stable environments may underestimate the actual flux by around 10%.

Table 8. Moving Average of Calculated Methane Flux, CCF, Wind Speed, and Wind Direction* for the Retrofit South Area

Loops	CCF	Flux (g/s)	Wind Speed (m/s)	Wind Dir (deg)
1 to 4	0.976	13	3.30	11
2 to 5	0.937	20	3.96	3
3 to 6	0.924	24	4.06	360
4 to 7	0.939	22	4.12	328
5 to 8	0.931	20	3.94	348
6 to 9	0.941	25	3.88	1
7 to 10	0.968	22	3.75	17
8 to 11	0.954	22	3.52	17
9 to 12	0.986	21	3.57	345
10 to 13	0.992	17	3.71	338
11 to 14	0.981	15	3.41	329
12 to 15	0.991	19	3.57	344
13 to 16	0.989	19	3.70	15
Average	**0.962**	**20**		
Std. Dev. of Mean	**0.0253**	**3.40**		

*wind direction shown is the angle from a vector normal to the plane of the configuration

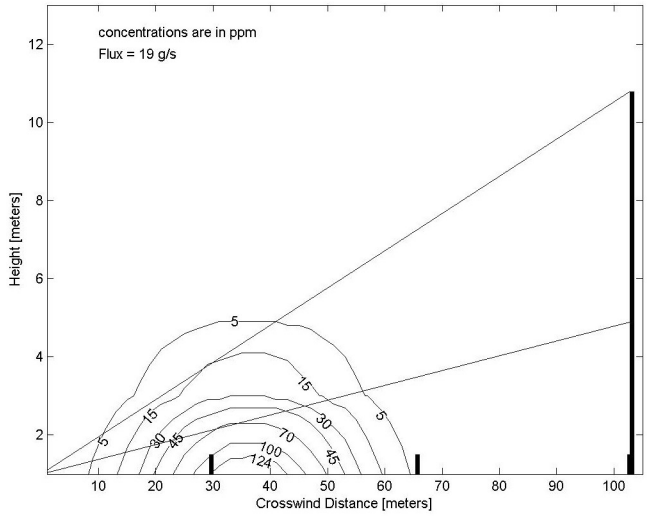

Figure 13. Reconstructed average methane plume from the moving average of loops 1 to 4 of the Retrofit North Vertical Scanning Survey

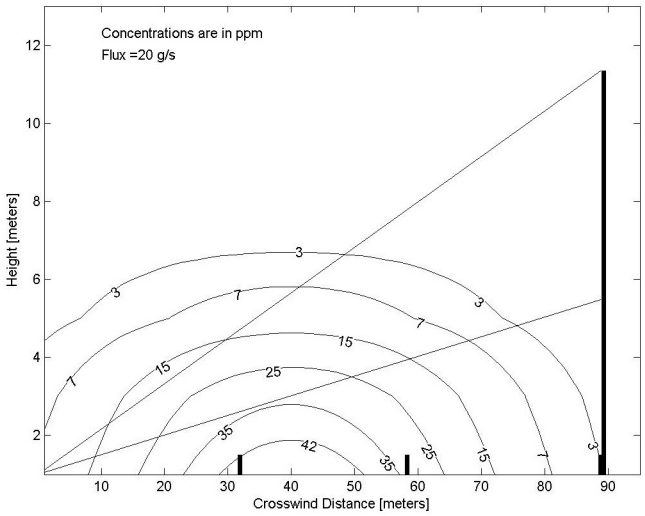

Figure 14. Reconstructed average methane plume from the moving average of loops 5 to 8 of the Retrofit South Vertical Scanning Survey

3.2.3 Control Area

Methane fluxes were calculated in the Control Area for instances when westerly winds were observed. Table 9 presents calculated Control methane fluxes. The first column of these tables refers to a running average calculation from the several "loops" of data collected. The second column shows the calculated CCF. The third, fourth, and fifth columns show the calculated methane flux (in grams per second), and the average wind speed and wind direction during the time the measurements were taken, respectively. The methane concentrations used to create these tables can be found in Table B-8 of Appendix B.

Table 9. Moving Average of Calculated Methane Flux, CCF, Wind Speed, and Wind Direction* for the Background Vertical Scan of the Control Area

Loops	CCF	Flux (g/s)	Wind Speed (m/s)	Wind Dir (deg)
1 to 4	0.973	6.0	0.95	332

*wind direction shown is angle from a vector normal to the plane of the configuration

Figure 15 presents the reconstructed methane plume from the vertical scanning survey of the Control Area. Contour lines give methane concentrations in ppm. The average calculated methane flux was 6 grams per second for the upwind survey.

In addition to measuring methane concentrations and methane flux, analysis was done to measure emissions of ammonia and VOCs from the Control Area. Concentrations of various compounds were calculated from the surface scan (mirror 1), and vertical scan (mirrors 2, 3, 4, and 5) experiments. Tables 10 and 11 present concentrations and calculated fluxes (in g/s) of VOCs and ammonia measured during runs 1 and 2,

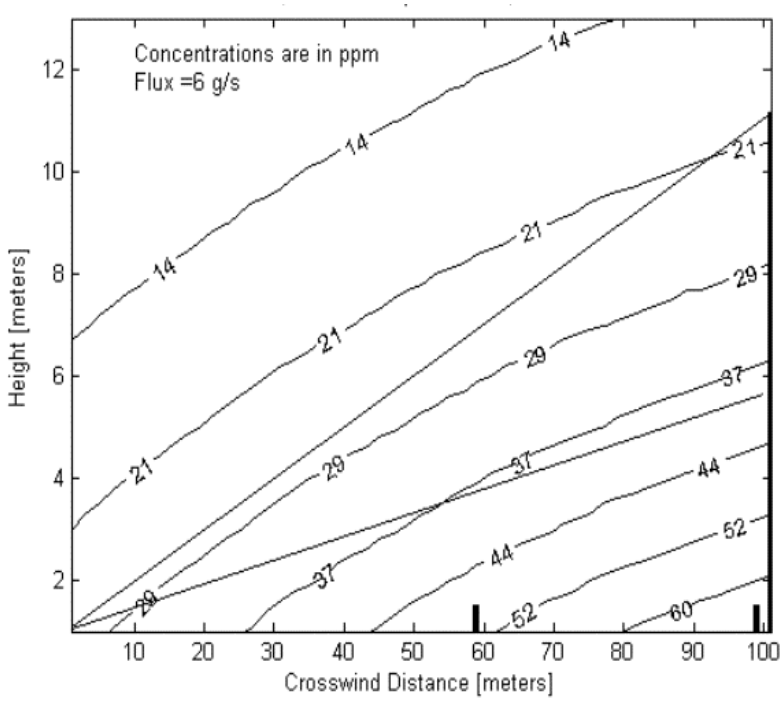

Figure 15: Reconstructed average methane plume from the Control Area Vertical Scanning Survey

respectively, of the Control vertical scanning survey. The fluxes were calculated by ratioing the measured methane concentrations with the measured VOC concentrations.

3.2.4 Biocover Area

Methane fluxes were calculated at the Biocover Area for instances where the vertical configuration was downwind of the actual survey area. Table 12 presents calculated methane fluxes measured at the site. The first column of these tables refers to a running average calculation from the several "loops" of data collected. The second column shows the calculated CCF. The third, fourth, and fifth columns show the calculated methane flux (in grams per second), and the average wind speed and wind direction during the time the measurements were taken, respectively. The methane concentrations used to create these tables can be found in Table B-8 of Appendix B.

Figure 16 presents the reconstructed methane plume from the vertical scanning survey of the Biocover Area. Contour lines give methane concentrations in ppm. The average calculated methane flux for the Biocover Area was 24 grams per second. No other compounds were detected in the Biocover Area

In order to analyze the results of the flux measurements, a comparison of methane flux calculations and wind data was made. Figure 17 presents a time series of methane flux and wind direction, for instances when the vertical configuration was located downwind of the survey area (the data used to create this graph can be found in Table B-8 of Appendix B). There appears to be a relationship between calculated methane flux and observed wind direction. The highest methane concentrations occur shortly after the observed wind direction has a northeasterly component (indicated as a wind direction of –30° to –40° in the figure). This

suggests that methane is being transported through the vertical configuration, from a "hot spot" located somewhere to the northeast of the Biocover Area.
Observed wind directions during the Biocover Area vertical scanning survey were highly variable. This is indicative of an unstable environment. This suggests that the calculated methane flux values could be underestimating the actual methane flux values in this area [*Hashmonay et al.*, 2001].

Table 10. Average Concentration and Calculated Flux of VOCs, Ammonia, and Methane for Control Area Vertical Scan-Run 1

Compound	Minimum Detection Level (ppmv)	Average Concentration (ppmv)	Flux (g/s)
TFM*	0.0018	0.0051	0.0036
CFM*	0.0098	0.034	0.015
Ethanol	0.0107	0.104	0.025
MTBE*	0.0108	0.046	0.019
Ammonia	0.0036	0.0202	0.0018
Methane		66.5	6

*TFM= Trichlorofluoromethane

*CFM= Chlorodifluoromethane

*MTBE= methyl tert-butyl ether

Table 11. Average Concentration and Calculated Flux of NMOCs for Control Area Vertical Scan-Run 2

Compound	Minimum Detection Level (ppmv)	Average NMOC Conc (ppmv)	NMOC Flux (g/s)
Ethylene	0.0041	0.0083	0.0014
CFM*	0.0097	0.031	0.016
Ethanol	0.0099	0.065	0.018
MTBE*	0.0101	0.037	0.019
Ammonia	0.0026	0.019	0.0019
Methane		57	5

*CFM= Chlorodifluoromethane

*MTBE= methyl tert-butyl ether

Table 12. Moving Average of Calculated Methane Flux, CCF, Wind Speed, and Wind Direction* for the downwind vertical scan of the Biocover Area

Loops	CCF	Flux (g/s)	Wind Speed (m/s)	Wind Dir (deg)
1 to 4	0.981	27	1.13	332
2 to 5	0.994	22	1.06	341
3 to 6	1.000	18	0.87	349
4 to 7	1.000	17	0.67	354
5 to 8	1.000	16	0.83	327
6 to 9	1.000	15	0.99	320
7 to 10	0.996	18	1.19	355
8 to 11	0.990	19	1.37	348
9 to 12	0.994	18	1.45	347
10 to 13	0.983	15	1.35	19
11 to 14	0.994	18	1.28	348
12 to 15	0.985	16	1.07	356
13 to 16	0.980	16	0.89	2
14 to 17	0.976	17	0.83	333
15 to 18	0.966	22	1.10	324
16 to 19	0.973	25	1.62	314
17 to 20	0.974	36	2.70	316
18 to 21	0.979	35	3.30	346
19 to 22	0.983	23	3.58	356
20 to 23	0.984	24	3.89	3
21 to 24	0.975	28	3.03	355
22 to 25	0.982	12	3.31	317
23 to 26	0.996	25	3.62	315
24 to 27	0.999	27	3.68	319
25 to 28	1.000	25	4.39	321
26 to 29	0.997	32	4.67	329
27 to 30	0.931	45	4.97	334
28 to 31	0.936	37	4.88	339
29 to 32	0.949	34	4.68	337
30 to 33	0.953	33	4.12	338
31 to 34	0.992	28	3.92	6
32 to 35	0.993	28	3.97	4
Average	0.932	24		
Std. Dev. of Mean	**.0183**	**7.96**		

*wind direction shown is angle from a vector normal to the plane of the configuration

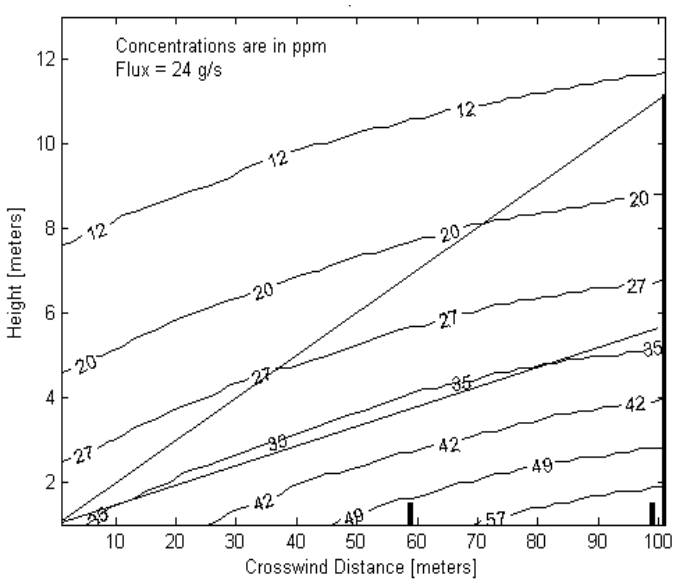

Figure 16. Reconstructed average methane plume from the moving average of loops 20 to 23 of the Biocover Vertical Scanning Survey

3.2.5 Compost Area

The methane concentrations found in this area are presented in the Tables B-10 and B-11 of Appendix B. The results of the Compost Area survey show that the average methane concentrations found were higher in the upwind area than in the downwind area. The survey did not detect any methane plume originating from the compost piles, which was expected. Due to these findings, we conclude that the Compost Area is not a source of methane at the site. Additionally, no other compounds were detected at the Compost Area.

3.2.6 Upwind Measurements

Throughout the period of optical scanning measurements, USEPA personnel set up and operated a bistatic OP-FTIR separate instrument in an upwind location, using a classical non-scanning configuration. Data collected by this instrument are representative of background concentrations from ambient, or upwind, sources. Background data were collected in each of the survey areas (refer to Figures 5, 6, 7, 8, and 9 for the location of the bistatic OP-FTIR configuration, which is denoted by the orange lines). Due to instrumentation problems, background OP-FTIR data is only available from the As-Built and Compost Areas. However, analysis of the surface scanning data from the Retrofit Area provides some information on background methane concentrations in this portion of the landfill.

The background survey from the As-Built Area found an average background methane concentration of 8.6 ppmv. Figure 5 shows that the bistatic OP-FTIR configuration was located along the western boundary of the As-Built Area, and the observed mean wind direction was from the northeast. Due to this, we can determine that the average background methane concentration found was probably indicative of a true background methane measurement for the As-Built Area.

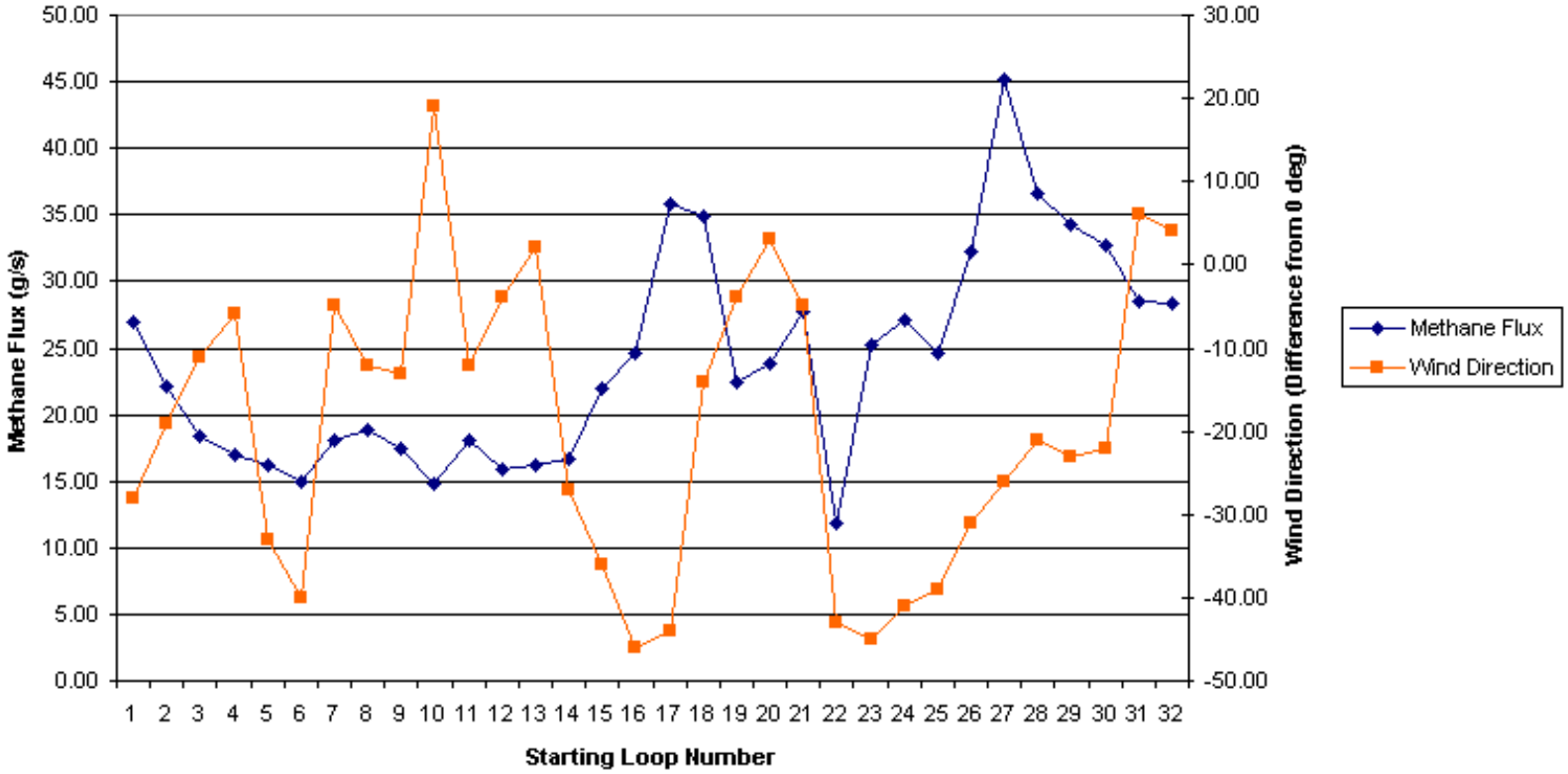

Figure 17: Time Series of Calculated Methane Flux vs. Measured Wind Direction for the Biocover (using moving average of 4 loops)

As mentioned above, the background OP-FTIR data from the Retrofit Area was unavailable due to instrumentation problems. However, in looking at the boundaries of the surface radial scanning results (Figure 12), one can estimate the background concentrations to be about 10 ppmv.

The background survey from the Compost Area found an average background methane concentration of 5.1 ppmv. This background value is very similar to the values detected immediately downwind from the compost piles, reinforcing the conclusion that no methane is emitted from the piles.

3.3 Data Quality Assurance and Control

In preparation for this project, a Category III Quality Assurance Project Plan (QAPP) was prepared and approved prior to the field campaign. In addition, standard operating procedures were in place during the survey, and the study was audited in the field and during post analysis.

3.3.1 Assessment of DQI Goals

The critical measurements associated with this project and the established data quality indicator (DQI) goals in terms of accuracy, precision, and completeness are listed in Table 1 of this document. Assessment of these measurements is discussed in the following subsections.

3.3.2 Meteorological/Theodolite Data

The Climatronics meteorological heads (which are used to collect wind direction, wind speed, ambient temperature, barometric pressure, and relative humidity), and the theodolite have recently been calibrated. The calibration of all instruments used to collect both critical and non-critical measurements should have occurred prior to the current field campaign.

Although calibration of the Climatronics heads did not occur prior to the field study, both Climatronics heads were calibrated in March 2003 by the USEPA/APPCD Metrology Lab (the last calibration of both heads occurred in November 1999). All functions were checked during the March 2003 calibration, and the only adjustment made was approximately a 4 degree change to wind direction for one of the Climatronics heads. As shown in Table 1, accuracy within 5% is an acceptable range, and this variance will have very little bearing on the final flux estimate.

It should also be noted that the wind direction measurement is not as critical to the flux estimates as the wind speed measurement. Additionally, checks for agreement of the wind speed and wind direction measured from the two heads (2m and 10m) were done. While it is true that some variability in the parameters measured at both levels should be expected, this is a good first-step check for assessing the performance of the instruments.

The Climatronics meteorological heads used in the current study were also used as part of a validation study [*Hashmonay et al., 2001*], and a study done in October, 2002 to measure fugitive emissions at a Region I Landfill in New Hampshire. In both controlled release studies, calculated emission rates were within 65-96% of the actual controlled release rate. The wind measurements taken during these studies provided good flux calculations and therefore were representative of the wind field in the whole vertical plane. Due to these factors, we feel that the accuracy and precision of the Climatronics heads, as stated in the QAPP and by manufacturer's specifications, are sufficient to provide favorable results using this method.

It has been determined that the accuracy of the measured optical path-lengths (which are collected using the theodolite), as stated in the QAPP and by the manufacturer's specifications, are not crucial to our method. However, calibration of the theodolite was done in the field during May 2003. The optical path-length was checked by measuring a standard distance of 50 feet (15.24 meters). The same distance was measured twice using the theodolite, and yielded distances of 15.43 and 15.39 meters. These results fall well within the acceptable accuracy range

stated in Table 1. The horizontal angle was checked by setting up two targets approximately 180° apart, measuring the two horizontal angles between the targets, and summing these values. The sum of the two values should be 360°. These angles were measured twice using the theodolite. The first test yielded a sum of 359°21'18", and the second test yielded a sum of 359°59'55". Both of these values fall well within the acceptable accuracy range stated in Table 1.

3.3.3 OP-FTIR Measurements

As a QC check of the accuracy of the OP-FTIR, we have verified the measurement of the known atmospheric background nitrous oxide concentration of around 320 ppbv from data taken with the monostatic OP-FTIR. It should be noted that 320 ppbv is an average value, as the atmospheric background value exhibits a slight seasonal variation. The data was taken from a sample of the actual data collected during the current field campaign. The average nitrous oxide concentration found was 311 ± 36.24 ppbv. The average value falls within the accuracy goal of 5%.

Additionally, we follow DQI procedures for proper operation as described in EPA Compendium method TO-16, and the OP-FTIR EPA Guidance Document. However, TO-16 is somewhat of an outdated method that does not fully address the issue of non-linearity. Since the completion of the TO-16 document, significant research has been performed by APPCD researchers to improve analysis over a wide range of concentrations [*Childers et al.*, 2001]. Application of the newly developed Non-Lin® software (developed by Spectrosoft) will provide better response of the OP-FTIR technique to higher levels of concentrations [*Childers et al., 2002*].

Tracer release is the ultimate DQI for confirming the RPM method as a whole system. Approximately three weeks after completion of the current study, another study was done using the ORS-RPM method at another site. During this study, a tracer release was done using ethylene. The same instrumentation used in the current study was used during this study. Ethylene was released through a soaker hose configuration located directly west of the vertical scanning survey. The wind direction during the time of the release was almost due west, which allowed the vertical configuration to capture the plume from the tracer release. The soaker hoses were set up in an "H" configuration to simulate an area source. The approximate dimensions of the "H" configuration were 10 meters wide, and 40 meters long (on each side). The weight of the ethylene cylinder was recorded prior to release of the gas, and immediately after the release was completed, using a digital scale. In addition, the precise starting and ending time of the release was recorded in order to calculate the average actual flux of ethylene. This flux value was then compared to the ethylene flux calculated from the vertical scanning survey.

The emission flux through the vertical measurement plane, calculated from the area integration of the concentration profile multiplied by the component of the wind speed normal to the vertical plane was determined as 0.98 g/sec. Since the measurement plane captured the entire plume, the entire flux through the plane is the emission rate of ethylene.

The ethylene tracer gas was released for 75 minutes. During this period, the measured mass of the ethylene cylinder was reduced by 4.59 kg. A loss of 4.59 kg over a 75-minute period indicates an average flow rate of 1.02 g/sec. The measured emission rate agrees with this mass-loss determination to 3.9 percent.

The flux of the ethylene release determined by mass-loss agrees well with the average ethylene flux calculated from the vertical scanning survey. Observed wind directions during the vertical scanning survey were not highly variable. This would be indicative of a stable atmosphere. *Hashmonay et al.* [2001] found that fluxes calculated during stable environments underestimated

the actual flux by around 12 %. The average ethylene flux calculated during the current experiment underestimated the actual average ethylene flux by 3.9 %.
In addition to verifying data collected with the OP-FTIR instruments a process audit was done by personnel not involved in the data analysis process, to verify that the transfer of data was done accurately. The audit consisted of verifying that concentration data provided by USEPA personnel, as well as wind speed and direction data were input into the reconstruction programs accurately. The results of the audit showed that this process was indeed done accurately.

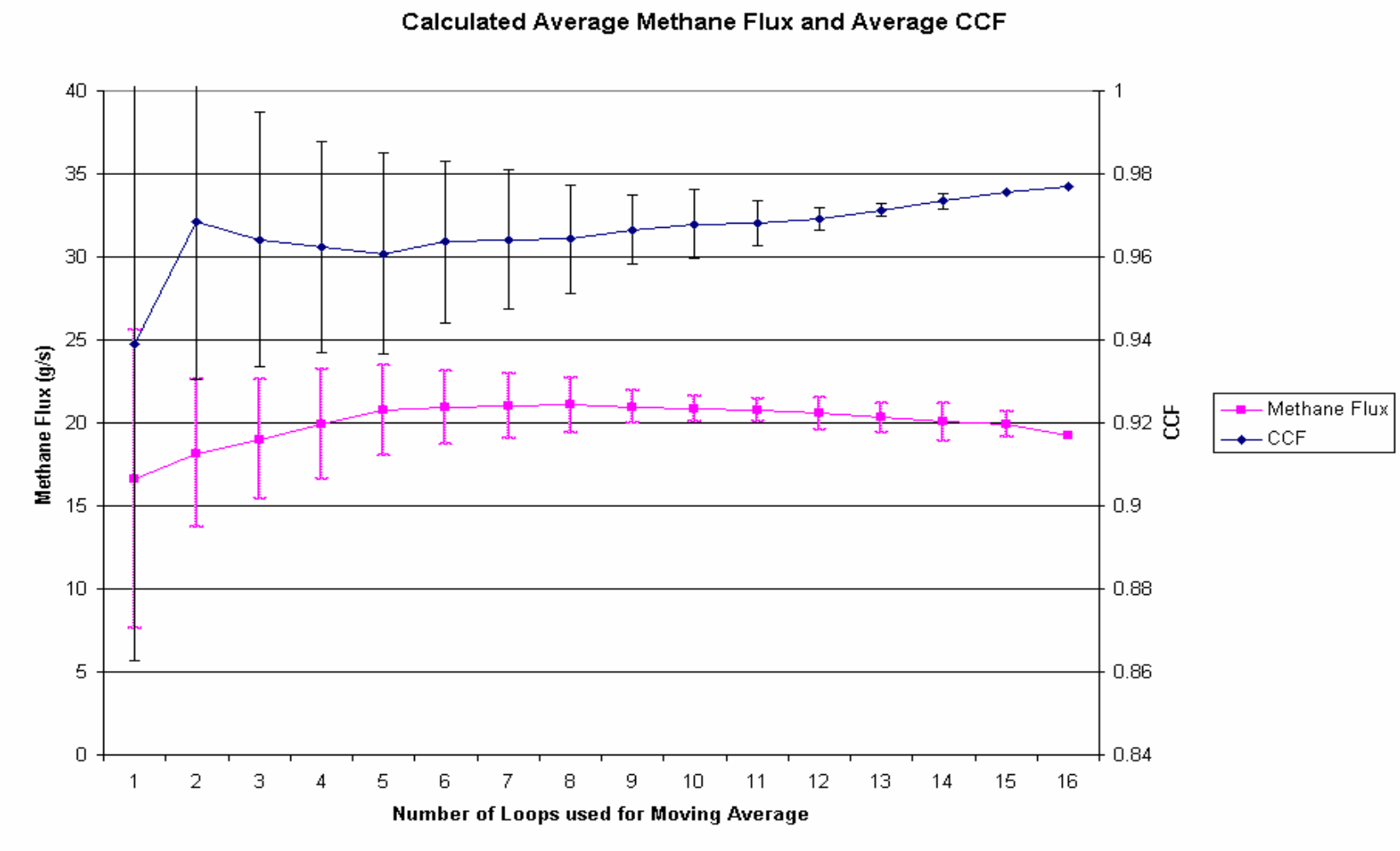

Figure 18. Calculated Average Methane Flux and Average CCF from the Retrofit South Vertical Scanning Survey

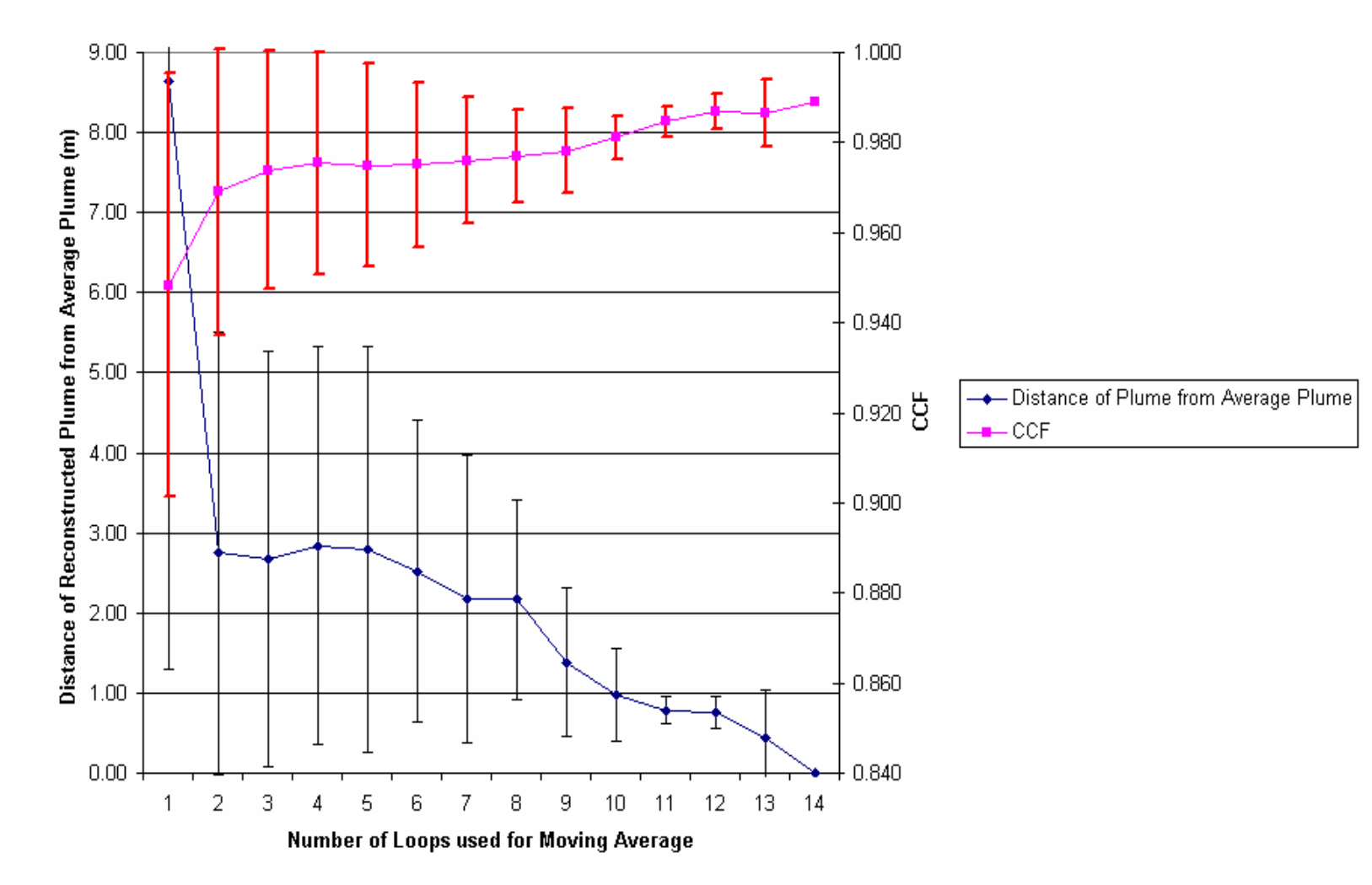

Figure 19. Distance of the Reconstructed Plume from the Average Plume, and Average CCF for the Retrofit North Area Radial Scanning Survey

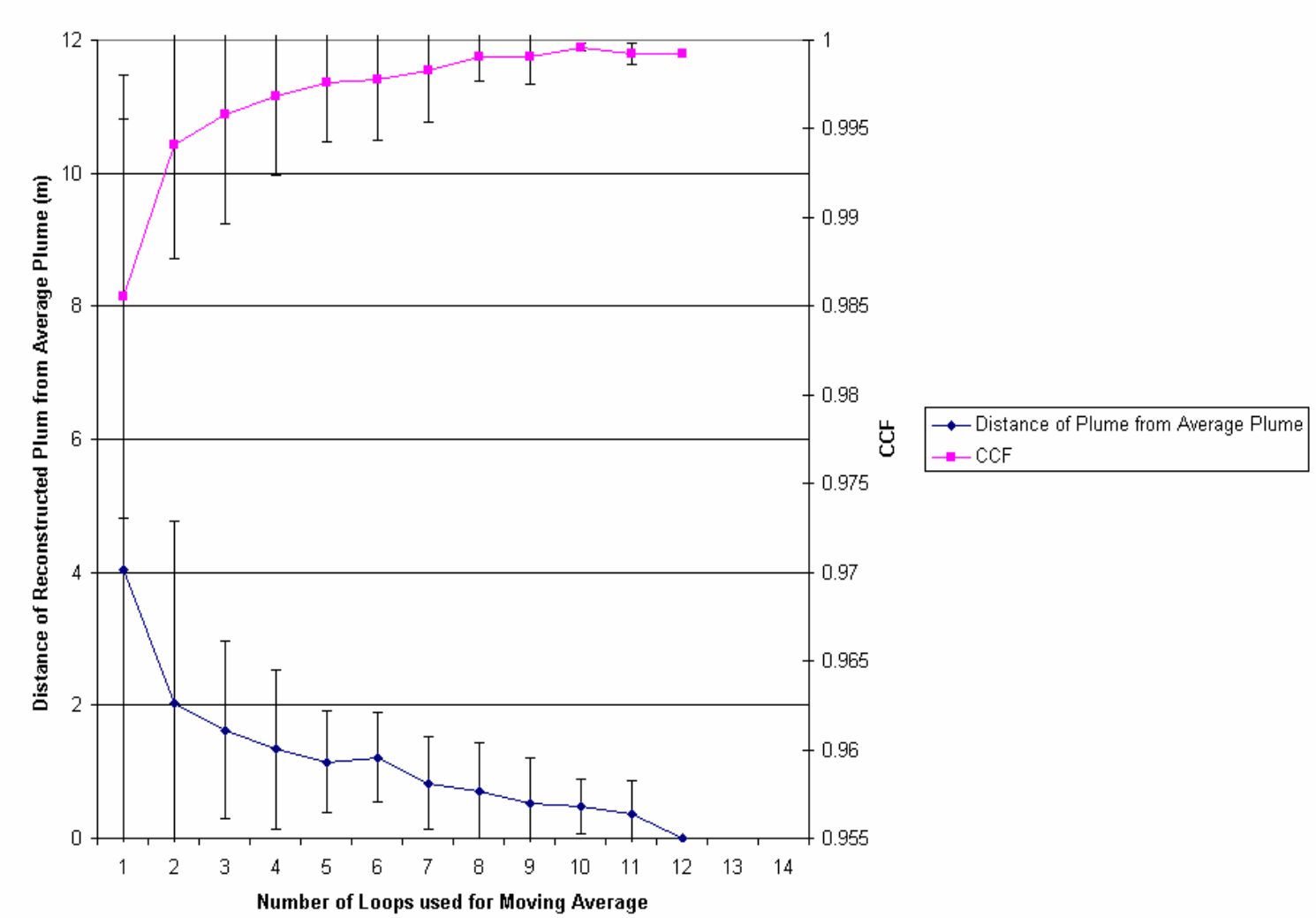

Figure 20. Distance of the Reconstructed Plume from the Average Plume, and Average CCF for the Retrofit South Area Radial Scanning Survey

3.3.4 Problems Encountered and Data Limitations

During the course of the field campaign, the project ran into some instrumentation problems and limitations, which slightly hindered some aspects of the data collection process. These included geographic barriers at the site, limitations in the optical range of the OP-FTIR instrument, and scanner errors that occurred primarily in the Retrofit Area.

The optical range of the OP-FTIR instrument used in this study was approximately 200 meters. The optical range is affected by many factors such as weather conditions, and topography at the site. This limitation primarily affected measurements taken in the As-Built Area. As mentioned in Section 3.1, the vertical scanning survey was oriented along the southern boundary of the survey area. Because of the limitation in the optical range of the OP-FTIR, it was not possible for the configuration to include the entire southern boundary of the As-Built Area. Due to this, it is probable that the calculated methane flux from the As-Built Area may be underestimating the actual flux. More advance OP-FTIR instruments can easily have a range of 500m in similar conditions.

Scanning errors occurred when the actual scanner (used to scan the OP-FTIR between each retroreflector in a configuration) stopped scanning. When this problem occurred, it prevented the completion of the survey, and the scanning program had to be reprogrammed. It is unclear what causes the scanning errors, but these errors occurred most frequently in the Retrofit Area, which may receive electromagnetic energy from air traffic as a result of it being located next to the airport and in the path of in-coming flights.

4 Conclusions

This report provides the first round of testing that is part of a longer-term effort to evaluate the performance of landfill bioreactor operations. The site has two different bioreactor operations (As-Built and Retrofit Areas). OP-FTIR measurements were conducted at the As-Built Area, where liquid additions are introduced at the work face. Sampling for this had to occur over the weekend when hauling operations were not active. The other type of bioreactor being evaluated is the Retrofit Area. This area was split into 2 different sections that were evaluated independently (north and south). In addition to evaluating the two types of bioreactors, the use of vegetative cover to reduce fugitive emissions (referred to as biocover) was evaluated. Emissions from the composting operation were also evaluated. Since this is an aerobic operation, methane emissions were not expected or found. Table 13 presents the average calculated methane fluxes, and the range of flux values, found at each area.

Table 13. Average Calculated Methane Flux (g/s) Found at Each Survey Area

Survey Area	Calculated Methane Flux	Range of Flux Values Calculated
As-Built	160 ± 27.3	118 to 180
Retrofit	39 ± 4.11	31 to 44
Control	6.0	6
Biocover	24 ± 7.96	12 to 45
Compost	N/A	N/A

The As-Built Area was found to have the highest methane fluxes, while the Control and Biocover Areas had the lower methane fluxes. The Compost Area was not found to be significant source of methane which one would expect since it is an aerobic operation.

In addition to vertical scanning, surface scanning was done in the As-Built Area and Retrofit Areas. Two definitive methane “hot spots”, having concentrations over 79 ppmv were found at the Retrofit Area.

5 References

American Society for Testing and Materials (ASTM), Standard Practice for Open-Path Fourier Transform Infrared Monitoring of Gases and Vapors in Air, E 1982-98.

ASTM, Standard Guide for Open-Path Fourier Transform Infrared Monitoring of Gases and Vapors in Air, E 1865-97, reapproved 2002).

Childers, J.W., E.L. Thompson, D.B. Harris, D.A. Kirchgessner, M. Clayton, D.F. Natschke, and W.J. Phillips, Multi-pollutant concentration measurements around a concentrated swine production facility using open-path FTIR spectrometry, *Atmos. Environ.*,35, 1923-1936, 2001.

Childers, J.W., W.J. Phillips, E.L. Thompson, D.B. Harris, D.A. Kirchgessner, D.F. Natschke, and M. Clayton, Comparison of an innovative nonlinear algorithm to classical least-squares for analyzing open-path Fourier-transform infra-red spectra collected at a concentrated swine production facility, *J. Appl. Spectr.*, 56, 3, 325-336, 2002.

Hashmonay, R.A., and M.G. Yost, Localizing gaseous fugitive emission sources by combining real-time optical remote sensing and wind data, J. Air Waste Manage. Assoc., 49, 1374-1379, 1999A.

Hashmonay, R.A., and M.G. Yost, Innovative approach for estimating fugitive gaseous fluxes using computed tomography and remote optical sensing techiniques, *J. Air Waste Manage. Assoc.*, 49, 966-972, 1999B.

Hashmonay, R.A., D.F. Natschke, K.Wagoner, D.B. Harris, E.L.Thompson, and M.G. Yost, Field evaluation of a method for estimating gaseous fluxes from area sources using open-path Fourier transform infrared, *Environ. Sci. Technol.*, 35, 2309-2313, 2001.

Hashmonay, R.A., K. Wagoner, D.F. Natschke, D.B. Harris, and E.L. Thompson, Radial computed tomography of air contaminants using optical remote sensing, presented June 23-27, 2002 at the AWMA 95th Annual Conference and Exhibition, Baltimore, MD.

Hashmonay, R.A., M.G. Yost, and C. Wu, Computed tomography of air pollutants using radial scanning path-integrated optical remote sensing, *Atmos. Environ.*, 33, 267-274, 1999..

Hashmonay, R.A., M.G. Yost, D.B. Harris, and E.L. Thompson, Simulation study for gaseous fluxes from an area source using computed tomography and optical remote sensing, presented at SPIE Conference on Environmental Monitoring and Remediation Technologies, Boston, MA, Nov., 1998, in SPIE Vol. 3534, 405-410

Lindberg, S.E., and J.L. Price, Airborne emissions of mercury from municipal landfill operations: a short-term measurement study in Florida, *J. Air Waste Manage. Assoc.*, 49, 520-532, 1999.

Lindberg, S.E., D. Wallschläger, E.M. Prestbo, J. Price, and D. Reinhart, Methylated mercury species in municipal waste landfill gas sampled in Florida, USA, *Atmos. Environ.*, 35, 4011-4015, 2001.

Natschke, D.F., R.A. Hashmonay, K. Wagoner, D.B. Harris, E.L. Thompson, and C.A. Vogel, Seasonal Emissions of Ammonia and Methane from a Hog Waste Lagoon with Bioactive Cover, presented at International Symposium on Addressing Animal Production and Environmental Issues, Research Triangle Park, NC, Oct. 2001.
Russwurm, G.M., and J.W. Childers, *FT-IR Open-Path Monitoring Guidance Document*, 3rd ed.; Submitted by ManTech Environmental Technology, Inc., under contract 68-D5-0049 to the U.S. EPA, Human Exposure and Atmospheric Sciences Division, National Exposure Research Laboratory: Research Triangle Park, NC, 1999.
Thorneloe, S., U.S. EPA's Field Test Programs to Update Landfill Gas Emissions Data, Accepted for publication in proceedings of Sardinia 2003, Ninth International Waste Management and Landfill Symposium, October 6 – 10, 2003, Sardinia, Italy.
Thorneloe, S. and K. Weitz, Holistic Approach to Environmental Management of Municipal Solid Waste, Accepted for publication in proceedings of Sardinia 2003, Ninth International Waste Management and Landfill Symposium, October 6 – 10, 2003, Sardinia, Italy.
U.S. Environmental Protection Agency, *Compendium Method TO-16: Long-Path Open-Path Fourier Transform Infrared Monitoring of Atmospheric Gases*, prepared under Contract No. 68-C3-0315, WA No. 3-10, Center for Environmental Research Information-Office of Research and Development, US EPA, Cincinnati, Ohio, Jan. 1999.
Waste Management, Inc. news release, Waste Management signs agreement with EPA to research and develop landfill bioreactor, *Biocover Projects*, October 2000.
Wu, C., M.G. Yost, R.A. Hashmonay, and D.Y. Park, Experimental evaluation of a radial beam geometry for mapping air pollutants using optical remote sensing and computed tomography, *Atmos. Environ.*, 33, 4709-4716, 1999.
Yost, M.G., and R.A. Hashmonay, Mapping Air Contaminants Using Path-Integrated Optical Remote Sensing with a Non-Overlapping Variable Path Length Beam Geometry, *United States Patent Office*, Patent # US 6,542,242 B1, issued April 1, 2003.

Appendix A

Site Configurations

Table A-1. Standard Distance, and Horizontal and Vertical Coordinates of mirrors used for Vertical and Horizontal Scanning in the As-Built Area

Mirror Number	Standard Distance (m)	Horizontal Angle from North (deg)	Vertical Angle* (deg)
Vertical			
1	67.1	270	0
2	116	276	0
3	167	274	0
4	117	275	3
5	118	276	6
As-Built Lower Surface			
1	70.5	291	
2	79.8	60	
As-Built Upper Surface			
1	109	244	
2	110	121	

*Vertical angle shown is the angle from horizontal (positive values indicate elevation from the horizontal, negative values indicate descent from the horizontal).

Table A-2. Standard Distance, and Horizontal and Vertical Coordinates of mirrors used for Vertical Scanning in the Retrofit Area

Mirror Number	Standard Distance (m)	Horizontal Angle from North (deg)	Vertical Angle* (deg)
North			
1	29.7	4	0
2	65.7	13	0
3	102	8	0
4	103	7	2
5	104	8	6
South			
1	31.8	158	0
2	58.2	172	0
3	88.7	177	0
4	91.9	176	3
5	93.1	177	7

*Vertical angle shown is the angle from horizontal (positive values indicate elevation from the horizontal, negative values indicate descent from the horizontal).

TableA-3. Standard Distance, and Horizontal Coordinates of mirrors used for Radial Scanning in the Retrofit Area

Mirror Number	Standard Distance (m)	Horizontal Angle from North (deg)
North		
1	55.5	67
2	72.2	47
3	34.3	44
4	92.7	36
5	115	30
6	56.4	25
7	84.3	18
8	108.8	13
South		
1	89.1	181
2	69.7	175
3	52.2	163
4	104	160
5	84.7	154
6	34.1	143
7	67.5	142
8	55.7	125

Table A-4. Standard Distance, and Horizontal and Vertical Coordinates of mirrors used for Vertical Scanning in the Biocover and Control Areas

Mirror Number	Standard Distance (m)	Horizontal Angle from North (deg)	Vertical Angle* (deg)
1	109	36	0
2	59.8	2	0
3	99.8	0	0
4	100	359	3
5	101	0	6

*Vertical angle shown is the angle from horizontal (positive values indicate elevation from the horizontal, negative values indicate descent from the horizontal).

Table A- 5. Standard Distance, and Horizontal and Vertical Coordinates of configurations used for Vertical Scanning in the Compost Area

Mirror Number	Standard Distance (m)	Horizontal Angle from North (deg)	Vertical Angle* (deg)
Upwind			
1	39.3	183	0
2	103	185	0
3	133	184	0
4	135	182	1
5	136	183	3
Downwind			
1	23.4	325	0
2	49.8	330	0
3	51.9	325	4
4	52.8	328	8

***Vertical angle shown is the angle from horizontal (positive values indicate elevation from the horizontal, negative values indicate descent from the horizontal).**

Appendix B

Methane, Ammonia, and VOC Concentrations

Table B-1.Methane Concentrations (in ppm) found during the As-Built Vertical Scanning Survey

Loops	Mirror 1	Mirror 2	Mirror 3	Mirror 4	Mirror 5	Wind Speed (m/s)	Wind direction from normal to vertical plane (deg)	Comments
1	23.0	86.1	113	155	136	0.6	52	Loop Used
2	192	196	158	97.8	53.3	1.9	28	Loop Used
3	167	206	162	90.1	60.8	2.5	39	Loop Used
4	154	207	160	103	82.1	1.7	46	Loop Used
5	177	246	183	80.7	33.9	1.8	73	Loop not used-does not meet wind criteria
6	51.4	96.7	154	118	86.0	1.7	75	Loop not used-does not meet wind criteria
7	149	255	176	108	47.3	1.4	75	Loop not used-does not meet wind criteria
8	84.0	140	117	70.4	60.7	2.5	30	Loop Used
9	149	134	84.9	62.8	52.7	2.3	36	Loop Used
10	125	183	142	64.6	42.5	3.0	75	Loop not used-does not meet wind criteria
11	107	140	129	47.1	50.2	2.7	78	Loop not used-does not meet wind criteria
12	73.7	177	167	69.3	40.9	2.2	75	Loop not used-does not meet wind criteria
13	67.5	91.8	49.2	59.1	98.5	1.5	97	Loop not used-does not meet wind criteria
14	178	157	128	70.1	59.2	1.2	69	Loop Used
15	98.2	236	170	53.4	22.9	0.8	85	Loop not used-does not meet wind criteria

Table B-2. Concentrations of Methane and VOCs (in ppmv) Measured on Mirror 1 of the As-Built Lower Surface Scan

As-Built Lower			Conc. (ppmv)	
Mirror 1				
Loop	Methane	Acetylene	Ethanol	Straight-Chain HCs
1	26	0.038		
2	27			
3	21	0.031		
4	24			
5	31			
6	41			
7	32			
8	31			
9	31	0.033		
10	35			0.055
11	31			0.064
12	26	0.018		
13	21			
14	23		0.035	
15	29			
16	22		0.038	0.057
17	32			
18	23			
19	23			
20	23			
	Avg=28			

Table B-3. Concentrations of Methane, VOCs, and Ammonia (in ppmv) Measured on Mirror 2 of the As-Built Lower Surface Scan

As-Built Lower		Concentrations	(ppmv)		
Mirror 2				Straight-Chain	Bent-Chain
Loop	Methane	Ethanol	Ammonia	Hydrocarbons	Hydrocarbons
1	13		0.0095		
2	15		0.0086		
3	13				
4	22		0.0060		
5	22		0.0063		
6	17				
7	21		0.015		
8	21		0.012	0.022	
9	13				
10	23		0.0066		
11	19				
12	17		0.0058	0.017	
13	14	0.0075			0.014
14	11				
15	11				
16	18				
17	19	0.0074			
18	11		0.0055		
19	21		0.0063		
20	11	0.0095			
	Avg=17				

Table B-4. Concentrations of Methane and VOCs (in ppmv) Measured on Mirror 1 of the As-Built Upper Surface Scan

As-Built Upper			Concentration (ppmv*m)		
Mirror 1					
Loop	Methane	Ethylene	Acetylene	Ethanol	MTBE*
1	24		0.0098		
2	18	0.0082	0.028		
3	27	0.0082	0.024		
4	25				
5	32		0.0067		
6	19				
7	29				
8	33				
9	37				
10	28			0.0055	
11	29				
12	23				
13	29				
14	19			0.012	
15	26			0.015	
16	25			0.015	
17	31			0.021	
18	27			0.020	0.0047
19	25			0.022	
20	28	0.0082	0.019	0.025	
	Avg=27				

* MTBE = Methyl tert-butyl ether

Table B-5. Concentrations of Methane, VOCs, and Ammonia (in ppmv) Measured on Mirror 2 of the As-Built Upper Surface Scan

As-Built Upper		Concentrations			
Mirror 2					
Loop	Methane	Ethylene	Acetylene	Ethanol	Ammonia
1	26		0.0038		
2	21		0.00077		
3	27	0.0057	0.011		
4	24				
5	28				
6	15		0.0054	0.011	
7	39	0.0087	0.022	0.0078	
8	31		0.0036		
9	24		0.0041		
10	31				
11	16	0.0053	0.017		
12	13				
13	12				0.0038
14	22		0.0049		0.0035
15	35	0.0092	0.020	0.025	
16	24		0.011		
17	22				
18	27	0.0079	0.017		
19	33		0.012		
20	36		0.0072	0.011	0.0023
	Avg=25				

Table B-6. Methane Concentrations (in ppm) found during the Retrofit Radial Scanning Survey

Loops	Mirror 1	Mirror 2	Mirror 3	Mirror 4	Mirror 5	Mirror 6	Mirror 7	Mirror 8
Radial North								
1	52	26	68	21	57	49	63	48
2	36	31	52	36	62	26	30	25
3	41	24	83	28	51	43	41	61
4	52	25	77	28	80	53	49	35
5	47	19	57	29	49	40	29	42
6	48	22	50	29	49	32	23	36
7	15	19	27	25	61	18	34	25
8	46	11	63	37	67	36	33	57
9	43	24	64	41	49	30	19	41
10	10	4	29	25	69	20	31	24
11	45	15	53	27	50	31	51	55
12	22	26	37	34	61	26	56	25
13	12	28	52	25	66	17	46	36
14	40	16	38	34	59	39	26	28
Radial South								
1	67	54	38	32	33	45	53	50
2	40	71	48	26	28	28	53	61
3	36	76	45	52	29	39	32	50
4	52	94	54	35	53	32	45	67
5	36	50	49	46	37	31	44	63
6	36	63	46	34	50	23	32	45
7	31	48	53	34	18	39	37	37
8	42	83	46	37	41	42	38	38
9	25	53	45	32	32	32	40	33
10	15	41	48	29	25	32	28	35
11	18	58	44	29	44	32	37	36
12	22	36	41	23	27	36	30	31

Table B-7. Methane Concentrations (in ppm) found during the Retrofit Vertical Scanning Survey

Loop	Mirror 1	Mirror 2	Mirror 3	Mirror 4	Mirror 5	Wind Speed (m/s)	Wind Direction from normal to vertical plane (deg)	Comments
Retrofit North								
1	20.9	87.2	51.3	15.5	12.0	2.7	347	Loop Used
2	48.3	62.0	36.4	11.9	5.1	2.7	6	Loop Used
3	32.7	71.1	35.3	6.7	3.1	3.8	354	Loop Used
4	25.3	65.3	36.1	9.0	8.5	3.3	352	Loop Used
5	38.9	69.5	40.9	9.0	3.6	3.3	353	Loop Used
Retrofit South								
1	32.8	31.9	23.1	12.2	11.1	2.0	127	Loop not used-does not meet wind criteria
2	46.6	39.6	22.4	13.9	8.9	2.9	110	Loop not used-does not meet wind criteria
3	37.9	33.2	29.2	14.5	7.6	4.3	196	Loop not used-does not meet wind criteria
4	31.5	40.5	17.6	16.2	5.9	1.8	330	Loop Used
5	16.2	42.1	30.2	11.6	5.6	4.2	334	Loop Used
6	51.6	44.4	27.6	12.3	5.1	4.0	89	Loop not used-does not meet wind criteria
7	26.2	35.1	13.5	11.2	15.7	2.2	69	Loop Used
8	64.0	42.7	30.9	14.8	9.3	3.2	12	Loop Used
9	22.7	38.6	15.4	16.2	17.1	4.5	296	Loop Used
10	15.7	37.2	28.3	14.2	11.4	4.6	321	Loop Used
11	30.0	38.9	29.5	10.0	4.7	4.3	324	Loop Used
12	20.7	29.8	23.5	15.5	15.8	2.4	89	Loop not used-does not meet wind criteria
13	20.4	43.8	41.2	15.9	13.9	4.2	348	Loop Used
14	50.7	37.2	27.3	12.1	5.9	4.1	27	Loop Used
15	17.3	41.2	30.3	9.0	6.8	3.3	322	Loop Used
16	15.2	16.0	12.8	16.4	5.1	2.6	325	Loop Used
17	19.8	41.2	28.1	8.4	5.9	4.8	318	Loop Used
18	15.7	40.5	32.6	7.5	6.2	2.9	351	Loop Used
19	30.9	41.3	35.0	14.0	5.7	4.0	24	Loop Used
20	71.3	33.8	33.3	11.4	11.2	3.1	88	Loop not used-does not meet wind criteria
21	23.3	40.0	38.2	11.7	9.2	4.2	101	Loop not used-does not meet wind criteria
22	22.4	33.3	21.3	11.4	8.5	2.3	324	Loop Used
23	36.2	28.2	12.6	11.0	12.1	2.4	346	Loop Used

Table B-8. Methane Concentrations (in ppmv) from the Biocover/Control Area Vertical Survey

Loop	Mirror 1	Mirror 2	Mirror 3	Mirror 4	Mirror 5	Wind Speed (m/s)	Wind direction from North (deg)	Comments
1	32.1	43.7	64.3	45.6	45.6	0.8	326	Loop used for Control
2	37.8	40.4	58.8	55.0	48.0	1.0	51	Loop used for Biocover
3	28.6	46.6	97.1	18.6	12.3	1.2	23	Loop used for Biocover
4	15.7	26.9	42.6	12.2	13.0	1.1	2	Loop used for Biocover
5	8.39	25.8	28.8	19.9	10.9	1.4	48	Loop used for Biocover
6	16.5	67.3	50.5	34.0	10.8	1.7	15	Loop not used-does not meet wind criteria
7	50.0	37.1	46.5	28.2	24.6	1.0	340	Loop not used-does not meet wind criteria
8	53.0	33.3	39.2	23.6	17.8	1.5	344	Loop not used-does not meet wind criteria
9	39.1	29.6	70.1	28.6	35.2	1.3	15	Loop not used-does not meet wind criteria
10	15.3	43.1	56.4	29.3	28.4	0.5	151	Loop used for Biocover
11	17.8	50.5	46.6	27.1	17.2	0.6	233	Loop used for Control
12	13.6	33.0	38.8	40.9	23.9	0.8	84	Loop used for Biocover
13	31.3	38.5	35.4	30.4	18.5	0.4	54	Loop used for Biocover
14	21.0	42.2	52.7	34.9	21.2	0.8	74	Loop used for Biocover
15	33.0	32.9	56.6	23.2	20.7	1.1	31	Loop used for Biocover
16	19.5	30.3	50.1	21.2	19.0	1.4	4	Loop not used-does not meet wind criteria
17	22.8	32.4	46.9	24.0	21.3	1.3	230	Loop used for Control
18	20.8	26.4	47.9	35.2	15.6	0.7	58	Loop used for Biocover
19	23.7	39.6	38.6	27.0	12.2	1.4	58	Loop used for Biocover
20	15.4	29.5	36.3	18.4	19.7	1.2	113	Loop used for Biocover
21	10.5	23.2	33.0	21.4	20.3	1.0	208	Loop used for Control
22	15.8	41.3	61.5	28.5	19.2	1.3	36	Loop used for Biocover
23	9.40	26.3	43.7	16.2	11.7	1.5	33	Loop used for Biocover
24	13.9	24.4	36.3	22.4	16.9	1.0	106	Loop used for Biocover
25	17.7	32.3	44.4	28.6	19.5	0.9	65	Loop used for Biocover
26	19.9	37.0	37.0	21.6	22.7	0.6	66	Loop used for Biocover

Loop	Mirror 1	Mirror 2	Mirror 3	Mirror 4	Mirror 5	Wind Speed (m/s)	Wind direction from North (deg)	Comments
27	18.1	54.1	49.8	32.3	30.0	0.7	58	Loop used for Biocover
28	28.0	50.1	38.6	32.8	29.2	0.9	77	Loop used for Biocover
29	28.7	47.1	39.0	29.5	28.2	1.2	6	Loop not used-does not meet wind criteria
30	50.0	73.7	68.0	47.0	47.9	1.3	20	Loop not used-does not meet wind criteria
31	53.0	78.8	55.7	52.4	41.1	1.0	357	Loop not used-does not meet wind criteria
32	39.1	78.6	71.3	40.3	39.4	1.9	85	Loop not used-does not meet wind criteria
33	36.7	74.4	83.2	48.3	39.5	2.3	29	Loop not used-does not meet wind criteria
34	11.1	61.2	55.1	20.3	17.2	1.3	147	Loop not used-does not meet wind criteria
35	14.9	35.4	43.2	30.6	25.9	2.4	56	Loop not used-does not meet wind criteria
36	15.1	18.1	23.8	7.53	7.75	4.8	64	Loop not used-does not meet wind criteria
37	21.6	14.1	14.5	8.73	6.76	3.1	105	Loop used for Biocover
38	7.95	14.7	20.7	8.67	5.96	2.9	77	Loop used for Biocover
39	9.46	18.8	33.8	9.27	6.90	3.7	58	Loop used for Biocover
40	7.93	15.9	61.7	19.4	20.4	1.6	35	Loop used for Biocover
41	19.0	47.1	35.3	14.2	6.03	4.1	44	Loop used for Biocover
42	14.9	35.3	31.1	22.9	33.4	1.6	355	Loop not used-does not meet wind criteria
43	26.9	35.7	31.5	24.7	21.0	2.9	355	Loop not used-does not meet wind criteria
44	32.6	18.6	25.2	25.7	15.7	2.5	344	Loop not used-does not meet wind criteria
45	7.71	38.6	43.2	27.1	27.0	3.2	356	Loop not used-does not meet wind criteria
46	25.2	58.3	23.9	16.1	6.85	4.0	66	Loop used for Biocover
47	11.3	17.6	22.6	14.9	7.15	3.8	76	Loop used for Biocover
48	24.4	44.4	39.4	25.5	17.0	2.9	352	Loop not used-does not meet wind criteria
49	40.0	35.6	51.0	27.8	7.92	3.3	363	Loop not used-does not meet wind criteria
50	16.9	24.2	39.0	16.2	17.8	4.1	37	Loop used for Biocover
51	19.1	20.0	18.8	10.6	9.65	5.1	76	Loop used for Biocover
52	16.2	17.6	19.3	8.96	4.84	5.2	83	Loop used for Biocover

Loop	Mirror 1	Mirror 2	Mirror 3	Mirror 4	Mirror 5	Wind Speed (m/s)	Wind direction from North (deg)	Comments
53	15.7	19.3	25.2	9.90	15.4	3.7	79	Loop used for Biocover
54	25.3	27.6	24.0	12.4	12.4	3.8	60	Loop used for Biocover
55	14.8	38.4	52.4	34.8	17.5	3.0	20	Loop not used-does not meet wind criteria
56	19.3	21.1	26.5	11.3	8.84	4.4	67	Loop used for Biocover
57	16.6	17.4	16.6	10.9	5.72	3.2	86	Loop used for Biocover
58	32.7	24.3	29.5	15.2	9.83	3.0	107	Loop used for Biocover
59	13.8	27.3	27.3	11.0	10.8	4.0	49	Loop used for Biocover

Table B-9. Methane, Ammonia and VOC Concentrations (in ppmv) Measured on Mirror 1 of the Biocover Area

Biocover				Concentration (ppmv)			
Mirror 1							
Loop	Methane	TFM*	CFM*	Ethanol	MTBE*	Ammonia	Ethylene
1	51	0.0057		0.104		0.012	
2	54					0.0068	
3	41					0.023	
4	38					0.028	
5	42		0.035			0.026	
6	32		0.028			0.031	
7	38		0.031			0.021	0.0077
8	28					0.016	
9	16				0.0059		
	Avg=38					**.021**	

*TFM= Trichlorofluoromethane

*CFM= Chlorodifluoromethane

*MTBE= methyl tert-butyl ether

Table B-10. Methane Concentration (in ppmv) found at the Compost Downwind Area

Loop	Mirror 1	Mirror 2	Mirror 3	Mirror 4	Wind Direction
1	5.8	5.1	5.8	4.2	183
2	5.8	5.1	5.3	5.5	135
3	5.3	5.3	6.0	4.3	144
4	5.2	5.3	6.8	5.6	166
5	6.4	5.4	6.2	4.6	208

Table B-11. Methane Concentrations (in ppmv) found at the Compost Upwind Area

Loop	Mirror 1	Mirror 2	Mirror 3	Mirror 4	Mirror 5	Wind Direction
1	10	13	13	12	11	322
2	7.3	11	9.5	10	10	218
3	10	10	9.3	10	10	280
4	7.7	9.1	8.4	8.6	8.8	297
5	8.7	10	10	10	11	259
6	10	11	11	13	13	274
7	8.5	15	15	15	16	235
8	19	20	19	20	22	224
9	13	28	27	29	28	239
10	28	30	27	28	26	225
11	22	26	23	24	24	234
12	12	23	21	22	21	225
13	5.4	6.1	5.9	4.7	6.7	143
14	5.4	7.2	6.4	5.5	8.3	132
15	5.7	6.3	6.4	4.8	6.9	104
16	6.1	7.5	7.4	5.7	7.1	87
17	6.0	7.1	6.0	5.4	5.4	168
18	6.0	8.0	5.7	6.1	9.0	290